ISTANBUL TECHNICAL UNIVERSITY ★ GRADUATE SCHOOL OF SCIENCE ENGINEERING AND TECHNOLOGY

NUMERICAL AND EXPERIMENTAL INVESTIGATION OF THE IMPACT PERFORMANCE OF 3D LATTICES WITH NEGATIVE POISSON'S RATIO

M.Sc. THESIS

Altuğ ATAALP

Aeronautics and Astronautics Engineering Department

Astronautics and Aeronautics Engineering Programme

JUNE 2018

ISTANBUL TECHNICAL UNIVERSITY ★ GRADUATE SCHOOL OF SCIENCE ENGINEERING AND TECHNOLOGY

NUMERICAL AND EXPERIMENTAL INVESTIGATION OF THE IMPACT PERFORMANCE OF 3D LATTICES WITH NEGATIVE POISSON'S RATIO

M.Sc. THESIS

Altuğ ATAALP
(511151102)

Aeronautics and Astronautics Engineering Department

Astronautics and Aeronautics Engineering Programme

Thesis Advisor: Prof. Dr. Halit Süleyman TÜRKMEN

JUNE 2018

İSTANBUL TEKNİK ÜNİVERSİTESİ ★ FEN BİLİMLERİ ENSTİTÜSÜ

NEGATİF POİSSON ORANLI 3 BOYUTLU LATİSLERİN ÇARPMA DAYANIKLILIĞIN DENEYSEL VE SAYISAL İNCELENMESİ

YÜKSEK LİSANS TEZİ

Altuğ ATAALP
(511151102)

Uçak ve Uzay Mühendisliği Anabilim Dalı

Uçak ve Uzay Mühendisliği Programı

Tez Danışmanı: Prof. Dr. Halit Süleyman TÜRKMEN

HAZİRAN 2018

Altuğ ATAALP, a M.Sc. student of ITU Graduate School of Science Engineering and Technology student ID 511151102 successfully defended the thesis/dissertation entitled "NUMERICAL AND EXPERIMENTAL INVESTIGATION OF THE IMPACT PERFORMANCE OF 3D LATTICES WITH NEGATIVE POISSON'S RATIO", which he prepared after fulfilling the requirements specified in the associated legislations, before the jury whose signatures are below.

Thesis Advisor :	**Prof. Dr. Halit Süleyman TÜRKMEN** Istanbul Technical University	.....
Jury Members :	**Asst. Prof. Dr. Demet BALKAN** Istanbul Technical University	.....
	Asst. Prof. Dr. Özgür DEMİR Yıldız Technical University	.....

Date of Submission : 04 May 2018
Date of Defense : 06 June 2018

To my family,

FOREWORD

First of all I want to thank my family for their endless support to me during my whole education life. And I want to offer my special thanks to İlayda Memiş. Without their support I would not be where I am today.

Also I want to thank to my venerable thesis advisors, Prof. Dr. Halit Süleyman Türkmen and Prof. Dr. Ioannis Doltsinis. With the help of them, I overcomed the difficulties not only in Istanbul Technical University, but also in University of Stuttgart. I appreciate their precious comments and efforts on my thesis.

The support for this thesis has been provided by the Scientific and Technological Research Council of Turkey under Project Number 115M465.

June 2018 Altuğ ATAALP

TABLE OF CONTENTS

Page

ABBREVIATIONS

ABS	**:** Acrylonitrile Butadiene Styrene
ABSplus	**:** Acrylonitrile Butadiene Styrene plus
CFRP	**:** Carbon Fiber Reinforced Polymers
N	**:** Newton

SYMBOLS

ρ	**:** Density
υ	**:** Poisson's ratio
E	**:** Modulus of elasticity
E_{long}	**:** Modulus of elasticity in longitudinal direction
E_{trans}	**:** Modulus of elasticity in transverse direction
X_T	**:** Longitudinal tensile strength
X_C	**:** Longitudinal compressive strength
Y_L	**:** Transverse tensile strength
Y_C	**:** Transverse compressive strength

LIST OF TABLES

Page

LIST OF FIGURES

Page

NUMERICAL AND EXPERIMENTAL INVESTIGATION OF THE IMPACT PERFORMANCE OF 3D LATTICES WITH NEGATIVE POISSON'S RATIO

SUMMARY

Poisson's ratio is simply the ratio between strain values of any two directions. The Poisson's ratio tells many things about the deformation behaviour of the material and what should be expected from material under specific loading conditions. Generally materials have Poisson's ratio between 0 and 0.5, mostly around 0.3. The negative sign in front of the formula causes conventional materials to have positive value.

Conventional materials tend to expand in the transverse direction when they are under compressive loading in longitudinal direction. Also, they shrink in the transverse direction when they are under tensile loading in longitudinal direction. However, these load applications are just the opposite for the auxetic materials. They shrink when they are compressed in any direction, and they expand in all directions when pulled in any direction. This causes auxetic materials too have negative Poisson's ratio.

Normally there are not too many natural auxetic materials. There are only few examples such as, some ligaments of muscles and joints, tooth gum of some animals. Most of the auxetic materials are man made. Even if the raw material has positive Poisson's ratio, auxetic material can be produced from it. Generally, unique geometry is used to create auxetic material. Without the improving technology, the production of the complex shapes would be so hard to process. For this thesis study, 3D printer is used to produce complex and complicated geometries. Also, the technical devices are designed and produced according to the needs.

In this study, two auxetic and one conventional geometries are used. First they are designed in CAD software programme and then analysed in finite element programme. After obtaining required knowledge about their strengths and weaknesses, these geometries are produced from 3D printer. Then impact tests and edge crush tests are performed on them to see their responses. Comparison between numerical analyses and experimental results are done. The importance and promising features of auxetic materials are detailly analysed.

NEGATİF POİSSON ORANLI 3 BOYUTLU LATİSLERİN ÇARPMA DAYANIKLILIĞIN DENEYSEL VE SAYISAL İNCELENMESİ

ÖZET

Poisson orani, temel malzeme özelliklerinden olup, malzemenin herhangi bir yükleme altında nasıl tepki verdiğini göstermektedir. Temel olarak iki farklı eksendeki gerilmenin negatifine eşittir. Geleneksel malzemelerde bir eksende uzama olduğunda diğer eksenlerde küçülme gözlendiğinden, formüldeki eksi ifadesi ifade kolaylığı sağlamaktadır. Ayrıca, farklı kombinasyonlardaki eksenler için poisson değerleri bulunabilir (x-y,x-z,y-z).

Ökzetik(Ing. Auxetic) kelimesi Poisson oranı negatif olan malzemeleri ifade etmektedir. Geleneksel malzemelerin aksine kendine has bir geometrik şekle ve malzeme özelliklerine sahip olması, ökzetik malzemeleri ilgi odağı haline getirmiştir. Örneğin çekme kuvvetine maruz kalan bir cismin boyu kuvvetin uygulandığı eksen boyunca uzarken, diğer yönlerde kısalmaktadır. Bu da, poisson oranının tanımından ötürü pozitif bir orana sebep olmaktadır. Ökzetik malzemelerde ise bu durum tam tersidir. Çekme kuvvetine maruz kalan ökzetik bir malzeme hem kuvvetin uygulandığı yönde hem de diğer yönde genişlemektedir. Basma kuvveti altında ise kuvvetin uygulandığı yönde ve diğer yönlerde küçülmektedir. Kısaca ökzetik malzemeler, kuvvetin uygulandığı eksenden bağımsız olarak çekme kuvveti altında genişlemekte, basma kuvveti altında genişlemektedir.

Ökzetik malzemelerin avantajı tek bir fiber tanesi düşünüldüğünde daha iyi anlaşılacaktır. Pozitif poisson orana sahip (geleneksel özelliklere sahip) bir fiber çekme kuvvetine maruz kaldığında eksenel yönde daralacak ve epoksiden ayrılmaya başlayacaktır. Fakat ökzetik bir fiber cekmeye maruz kaldığında eksenel yönde de genişleyecek ve epoksiye daha iyi tutunarak kaymalara ve ayrılmalara engel olacaktır. Böylelikle daha dayanıklı bir kompozit elde edilmiş olacak ve daha yüksek şiddetteki kuvvetlere dayanabilecektir.

Oldukça yenilikçi olan bu konuda deneysel incelemelerin yapılması malzeme araştırmaları alanında oldukça ilgi cekmektedir. Ökzetik malzemelerin kendine has benzersiz malzeme özelliklerinden faydalanarak yenilikci ürünler üreterek askeri, savunma, ve havacılık alanlarında kullanılması oldukca olasıdır. Özellikle mermi ve ani basınç yüklemelerine karsi eksen ici ve eksen disi carpma dayaniklilikleri bu tez calismasinda da detayli olarak incelenmektedir.

Negatif poisson oranına sahip malzemeler doğada nadir olarak bulunmakla birlikte, genel olarak insanlar tarafından üretilmektedir. İnsan yapımı negatif poisson oranlı malzemeler, tüm ökzetik malzemeler arasında büyük çoğunluğu oluşturmaktadır ve geleneksel (pozitif poisson oranlı) bir malzemenin geometrisinin özel olarak tasarlanıp değiştirilerek ökzetik malzemeye çevrilmiş halidir. Bu malzemeler için maalesef geleneksel üretim yöntemleri kullanımı pratik değildir. Gelişen teknoloji ve üç boyutlu yazıcıların yaygınlaşması ile kolaylaşan üretim teknikleri, karmaşık geometrilerin üretilmesine de olanak tanımıştır. Bu çalışmada da ökzetik malzemelerin üretimi Infotron marka üç boyutlu yazıcıda yapılacaktır.

Üç boyutlu yazıcıdan üretilecek olan numunelerin bilgisayar kullanarak sayısal analizini yapmak deneysel ve sayısal değerlerin karşılaştırılmasına da olanak sağlamaktadır. Ayrıca üç boyutlu yazıcı sayesinde bilgisayarda analizi yapılan

parçanın birebir aynısının üretimi yapılabilmekte ve böylelikle bilgisayar analizi ile deneysel sonuçların karşılaştırılması yapılabilmektedir.

Bu çalışmanın birinci bölümünde Ökzetik malzemeler ile ilgili genel bir bilgi verilmiş, daha önceden yapılan çalışmalardan bahsedilmiştir. Ökzetik malzemeler, kendilerine has deformasyon mekanikleri sayesinde çok farklı araştırmanın konusu olmuşlardır. Bu araştırmalar ve genel olarak Poisson oranı hakkında bilgilendirilme yapılmıştır.

İkince bölümde ise, bu çalışma kapsamında yapılan sayısal analizler anlatılmıştır. Kullanılacak olan malzemelerin tasarımları, sayısal analizin yapılacağı programın tanımı ve sayısal modellerin bu programa aktarımlarından bahsedilmiştir. Sayısal analizin yapılması için gerekli olan bilgiler sırasıyla verilmiştir. Bu bilgilerden bazıları kullanılan parçaların eleman ve düğüm sayıları, parçaların birbiri arasındaki ilişki bilgileri, kullanılan malzeme özelliklerinin tanımlanması, ve çarpma etkisi için kullanılan parçanın hız bilgilerinin ve özelliklerinin tanımlanmasıdır.

Üçüncü bölümde öncelikle var olan test sistemleri tanıtılmıştır. Daha sonra bu çalışma için gerekli olan ve test sistemine entegre edilebilecek parçaların tasarımı ve bu parçaların üretimi gösterilmiştir. Daha sonra darbe testi anlatılmaya başlanmıştır. Darbe testi için kullanılması gereken alüminyumun kalınlık değerinin bulunması ve bu değer bulunduktan sonra üretilen numunelerin alüminyum ile kaplanması gösterilmiştir. Daha sonra numuneler test düzeneğine bağlanarak atışlar gerçekleştirilmiş ve gerekli değerler elde edilmiştir. Bu atışlar sayısal analiz sonuçları ile karşılaştırılarak analizlerin doğrulanması yapılmıştır.

Üretilecek ökzetik malzemeler öncelikle bilgisayar ortamında üç boyutlu olarak oluşturulmuşlardır. Bilgisayar ortamında Ls-Dyna analiz programı kullanılarak deneysel olarak test edilen numuneler için analizler yaptırılmıştır. Analizler farklı parçacık hızları, farklı kabuk kalınlıkları, ve farklı sayıdaki dış katman sayıları için tekrarlanmış ve incelemeler yapılmıştır. Analizler sonucu bulunan değerler yapılan testlerle karşılaştırılmıştır.

Bilgisayar ortamında analizi yapılan numuneler üretilerek deneysel testleri de yapılmış ve çıkan sonuçlar literatür ve analiz sonuçlarıyla karşılaştırılmıştır. Bilgisayar analizleri ve deneysel sonuçların doğruluğu açışından öncelikle kullanılan malzemelerin kupon testleri yapılmıştır. ASTM standartlarında belirtilen standartlara göre numuneler hazırlanarak gerekli testler yapılmış ve malzeme özellikleri elde edilmiştir. Daha sonra bu malzeme özellikleri bilgisayarlı analiz için temel özellik olarak kullanılarak analizler güncellenmiştir. Böylelikle deneylerde kullanılan malzemelerin özellikleri tam olarak öğrenilmiş ve bilgisayar analizleri gerçeğe yaklaştırılmıştır.

İlk olarak yapılan darbe analizinde üç farklı geometri kullanılarak farklılıkları ortaya konmuştur. Penetrasyon mesafesi, darbe yüklemesi için oldukça önemli bir konudur. Kritik durumlar için mesafe ölümcül olabilir ve mümkün olduğunca küçük bir nüfuz mesafesini korumak, darbe yüklemesi araştırmaları için ana konudur. Parçacık, bal peteği çekirdeğinde, reentrant çekirdekten daha fazla mesafe kat etmiştir. Ek olarak, darbe yükü sırasında meydana gelen maksimum stres değeri, balpeteği için daha yüksektir. Darbe yüklemesi için bir diğer önemli konu, malzemenin belirli bir deformasyon değeri altında kalması için daha az stres değerine sahip olmasıdır. Reentrant geometride daha küçük maksimum stres değerine sahiptir. Bu da reentrant geometrinin daha dayanıklı olduğunu göstermektedir.

Ezme testi, numunenin ezilme direncini görmek için önemlidir. Ayrıca bu testin en önemli beklentisi, ökzetik malzemenin sıkışma etkisini görmektir. Kendilerine uygulanan bir basma yüklemesi olduğunda, ökzetik malzemelerin genişlemek yerine daralarak sıkılaşması beklenmektedir. Bu olgu, birinci bşlümde girinti direncinin yardımıyla açıklanmaktadır. Ezme testi için bir reentrant ve bir anti tetrachiral numune hazırlanmıştır. Her iki numune de 4 mm uzunluğunda ve 4 mm genişliğinde ve 5 mm kalınlığındadır.

Her iki geometrinin de zamanla daha sıkılaştığı görülmüştür. Bu sadece malzemenin üzerine uygulanan basma kuvveti etkisinden kaynaklanmamaktadır. Ökzetik malzemelerin kendine has olan geometrisi dolayısıyla kaynaklanmaktadır. Anti-tetrachiral formda ökzetik etki daha belirgindir. Zaman geçtikçe, hücreler arasındaki boşluklar küçülmüştür ve numunenin genişliği azalmıştır. Bu etki, malzemenin daha güçlü olarak daha yüksek kuvvete dayanmasına yardımcı olmuştur.

Yapılan testler karşısında umut vaat eden bir görüntü sergileyen ökzetik malzemelerin uygulanabileceği çok değişik alanlar bulunmaktadır. Örneğin kurşun geçirmez yelek üretiminden tanklara, hava-uzay yapılarında koruyucu ek katman olarak kaplanmaya kadar değişik bir skalada uygulama alanı vardır. Özellikle havacılık alanındaki malzeme arayışına da cevap verebilecek bir malzemedir. Geleneksel malzemelerin aksine alışılagelmemiş bir deformasyon mekanizması olması ökzetik malzemeleri çekici yapmaktadır. Örneğin farklı koşularda farklı yüklemelere maruz kalan bir uçak parçası için ökzetik malzeme kullanılarak bir tasarım yapılabilir, veya geleneksel malzemeyle birlikte kullanılarak her türlü yükleme durumuna karşı daha güçlü hale getirilebilir.

1. INTRODUCTION

1.1 Introduction to Auxetic Materials

Most of the materials encountered everyday expands when we compress them. They also squeeze when they are pulled. This phenomenon is the nature of the conventional materials. However, the situation for auxetic materials is just the opposite of the described situation of conventional materials. The discovery of the materials with negative Poisson´s ratio led people to use them in various situations when conventional materials´ properties are not sufficient for those applications. The behaviour of the auxetic materials can be explained by following two states: When an auxetic material is under tensile loading in the longitudinal axis, it expands in the other planes. Likewise, when an auxetic material is under compression loading in the longitudinal axis, it shrinks in the other planes.

The word auxetic is used to describe the materials with negative Poisson´s Ratio. The first auxetic polyurethane foams are produced by Roderick Lakes in 1987 (K.E. Evans, 2000). Since their first discovery, materials with negative Poisson´s ratio attract interests of scientists all around the world. Recent researches on the materials are tend to focus on the auxetic materials as they react to the applied loads differently than conventional materials. However, still the resources about auxetic materials are limited. In this manner, both experimental and theoretical studies on auxetic materials are quite new. Auxetic materials are getting more common with the help of improved 3D printers. The effect of negative Poisson´s Ratio can be seen in Figure 1.1. Unlike the conventional materials, auxetic materials do not squeeze under the tensional loading. The shape of the material gives it the unique ability to react and the material expands under the tensile loading.

Deformation kinematics of the auxetic materials are shown with the arrows in the Figure 1.1. The structure is at rest and undeformed at the left image. Bigger arrows on the right image shows the direction of the applied load, in this case tensile loading. Smaller arrows imply the reaction of the structure. For this loading condition, auxetic

material expands under tensile loading whereas conventional materials are expected to shrink.

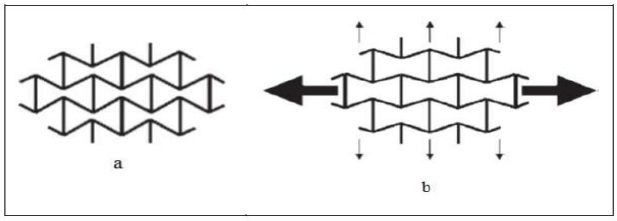

Figure 1.1: Effects of tensile loading on the auxetic materials. The states of auxetic materials before (a) and after (b) the load. (K.E. Evans, 2000)

Auxetic materials can be produced in many different shapes and dimensions with the help of increasing technological capability. Producing the desired auxetic material in nanometers or micrometers became easier with the improving 3D printers. The scale of the length of auxetic materials can be seen at Figure 1.2. Auxetic materials exist on a large scale of nanometers to meters, and they are convenient to most of the applications with their varying size.

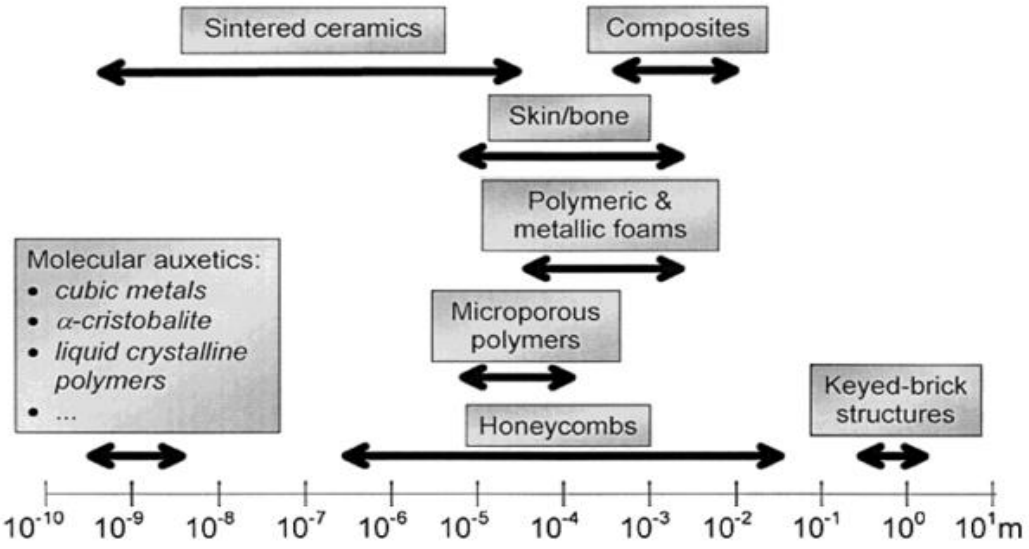

Figure 1.2: The length scale of the auxetic materials (Kenneth E. Evans & Alderson, 2000).

Even though the auxetic materials´ discovery is new, in nature there exists natural auxetic materials. Some of the animals´ skins (cat, salamander, cow), some of the joints of human body, iron pyrites and single crystal of arsenic are examples of natural auxetic materials that can be found in nature (A. Alderson & Alderson, 2007). Even if the material used in the production has a positive Poisson's ratio, the unique shape

causes created structure to have negative Poisson's ratio. One of the unique geometries is anti tetrachiral type. And since these materials with negative Poisson's ratio are produced according to some geometrical relations, they can be optimized to have better shape or better mechanical properties. G. E. Stavroulakis states that all materials have Poisson's ratio between -1 and 0.5, it is also expressesed further that these limits are in semidefinite form. Inverted hexagonal structures and noncovex microstructures are the most reasonable structures to examine the auxetic behaviour (Stavroulakis, 2005).

Some types of the auxetic geometry are simply derived from the conventional material geometry. An example for this type auxetic can be seen in Figure 1.3. The unique deformation property of the reentrant auxetic materials are coming from one simple geometrical ratio change. Normally all of the edges are equal to each other in hexagonal. M. Mir et al. states that this equality can change, which leads to reentrant structure (Mir, Ali, Sami, & Ansari, 2014). Newly created ratio is main subject of the optimization problem. By changing this ratio, one can have completely different mechanical properties. So this also means that the Poisson's ratio becomes directly proportional to the angle of the reentrant structure.

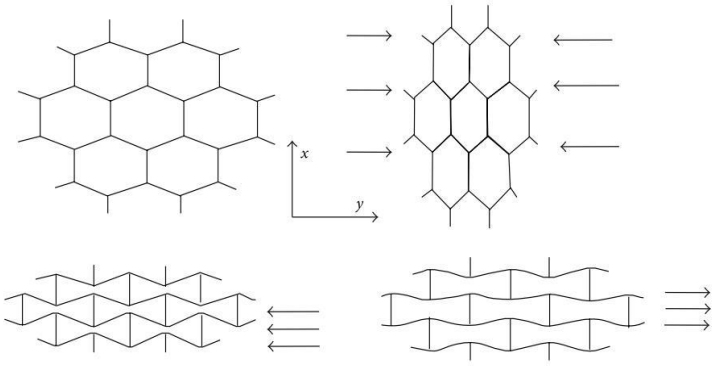

Figure 1.3: Deformation mechanics of conventional material (above) and auxetic type (reentrant) material (below) (Mir et al., 2014).

Also, unique properties of the auxetic materials can be used in very different ways such as crush box in vehicles. Accidents of the transport vehicles are quite common and this is one of the biggest reasons of the financial losses and even casualities. The general agreement of the society is decreasing the accident amounts strengthening the materials used in vehicles. Auxetic materials attract interest, because they are new and very promising in the subject of withstanding to the loading. They can be used as a

crash boxes in vehicles in order to increase the durability and toughness of the automobiles.

1.2 Advantages of Auxetic Materials to Conventional Materials

Auxetic materials have to be proven that they are better than the conventional materials just like every newly found material or structure. To prove the properties of materials with negative Poisson´s ratio, they must be tested and compared with conventional materials in every area. Therefore, there exist too many tests and comparisons of auxetic materials and conventional materials.

Auxetic materials are theoretically expected to have better shear modulus, fracture thoughness, acoustic response and most importantly indentation resistance (Mir et al., 2014). These properties of auxetic materials make them attractive for not only military applications, but also civil applications.

The comparison of the conventional and auxetic materials can be seen in Figure 1.4. At the same figure, how conventional and auxetic materials behave under indentation tests is also shown. It can be seen that unlike conventional materials, auxetic materials are expected to behave better under indentation loadings. The nature of auxetic materials allow them to expand under impact loading and to resist the loading. This advantage can be used in life vests or in transportation vehicles, like airplanes. They can be strengthened more when auxetic materials used and lives of innocent people can be saved.

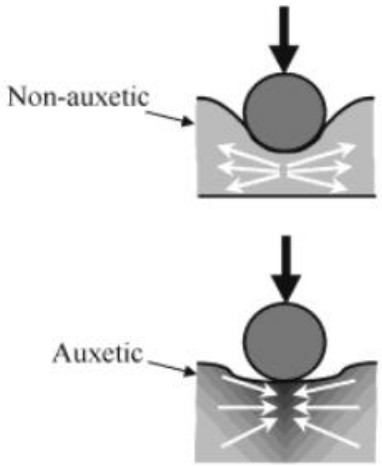

Figure 1.4: Indentation resistance comparison of auxetic and conventional material (Kenneth E. Evans & Alderson, 2000).

It can be seen from Figure 1.4 that, the parts of the material that is away from loadings´ effect gather under the load´s application point and the overall capacity of the material to withstand loading is increasing with that effect. However, nonauxetic material behaves like giving way to the applied loading and makes the material more vulnerable to bad damages.

K. L. Anderson et al. performed fibre pullout tests with Instron 4200 testing machine that is available up to 100 N load. The loading rate of the test was 5 mm/min, and the fibre length was 50 mm. The main aim of this experiment was to compare auxetic fibres and nonauxetic fibres. The comparison between auxetic and non auxetic fibers can be seen in Figure 1.5 (K. L. Alderson et al., 2005).

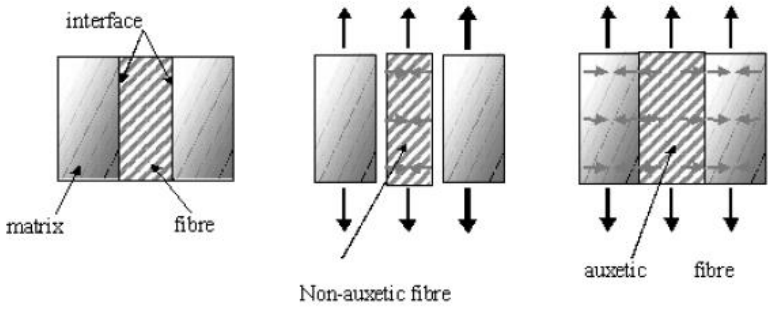

Figure 1.5: Auxetic materials´ reaction to pull force and comparison with the conventional materials(K. L. Alderson et al., 2005).

The results of the experiment K. L. Anderson et al. did can be seen at Figure 1.6, which is a plot of displacement versus applied force. If the graph is analyzed, it can be seen that auxetic fibres can withstand much greater forces under same amount of displacement. The peak values of force and energy are given by K. L. Anderson et al. as 0.96 N and 8.3 mJ for auxetic materials and 0.44 N and 2.5 mJ for nonauxetic materials (K. L. Alderson et al., 2005). Main reason of this phenomenon can be explained by using Figure 1.5. Auxetic fibres expand and hold on to matrix, and this increases the durability of the material under loading. Resisting the load without being deformed too much can be live saving for many situations. Undergoing more load and deforming less is one the most desired design criteria when human life is concerned.

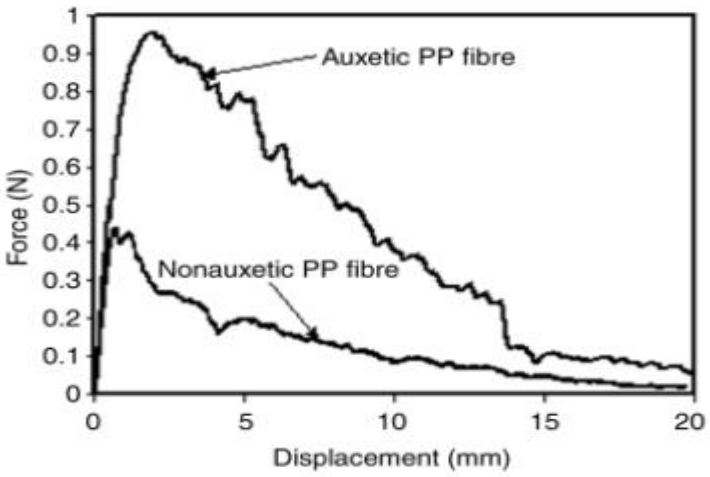

Figure 1.6: Displacement vs Force plot of auxetic fibres and nonauxetic fibres in the pull out test (K. L. Alderson et al., 2005).

Auxetic materials can also be used for indentation resistance or sound emittance capacity. They are also used to create coupling in piezocomposites. W. A. Smith suggests the application of the auxetic materials for piezocomposite couplings, and then looks for the optimizing the properties of them. It is also explained that the optimization problem of having flexibility, stability, electrical impedance matching as well as preserving the minimum weight. Also, maximum efficiency of electromechanical energy alteration is stated as the key point of design. In the final, auxetic materials are seen to improve the electromechanical properties of the piezocomposites (Smith, 1991).

J. Schwerdtfeger et al. analysed existing auxetic materials' production methods and decided to improve the auxetic structures by using optimization tools (Schwerdtfeger et al., 2011). They used solid isotropic material with penalization (SIMP) method to use topology optimization for auxetic materials. According to their claim, the results of the optimization process is superb in the numerical and measured results. Additionaly, they obtained serious improvement in the negative Poisson's ratio values by using the non intuitive modifications.

C. Qi, S. Yang, et al. performed numerical analyzes to test the ability of auxetic materials and to compare it with other materials. They used frames with 30° cell angle (regular), 0°cell angle (rectangular shaped) and -30° cell angle (auxetic) as a core of sandwich structure. Auxetic materials showed better withstanding to impact loadings among other analysed structures. According to C. Qi, S. Yang, D. Wang, and L. Yang´s

simulation results, this effect is seen better at relatively low impact velocities. At the Figure 1.7, it can be seen that the particle has moved less than the other simulated materials at the same amount of time. Even that small difference of propagation can make a huge difference for safety reasons. After seeing that auxetic materials´ better properties against other configurations, C. Qi et al. performed simulations on auxetic materials only with changing the face sheet thickness, density wall thickness and cell size. (Qi, Yang, Wang, & Yang, 2013)

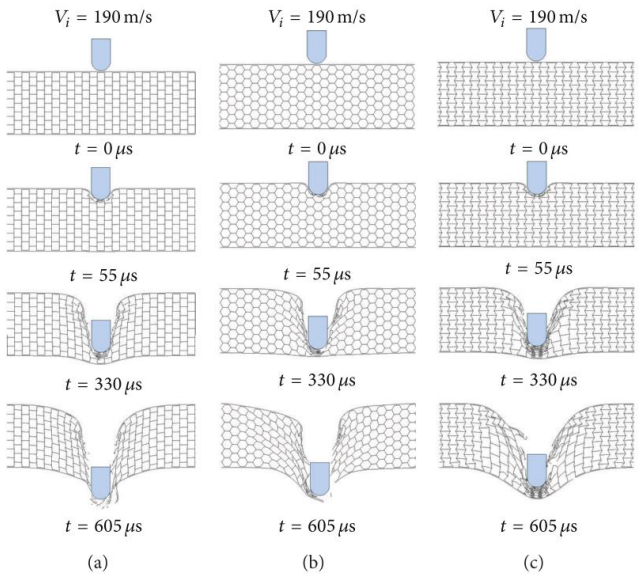

Figure 1.7: Simulation analysis of regular shaped rectangular shaped and auxetic frameworks under 190 m/s impact. a) rectangular shaped, b) regular shaped, c) auxetic shaped (Qi et al., 2013).

Another way of studying auxetic and conventional materials is the optimization methods. M. Ruzzene and F. Scarpa studied on their paper about optimization of band gap and aligned properties of both auxetic and honeycomb cells. Their main goal was to decrease the wave distinguishing capability of the structures. They also gave their design variables and objective functions in their optimization statement. They also analysed the results of the optimization process and evaluated the outcomes with respect to others (Ruzzene & Scarpa, 2005).

S. Czarnecki and P. Wawruch also studied topology optimization for auxetic materials (Czarnecki & Wawruch, 2015). Their approach is relied on Free Material Optimization method to search the optimum values that yields maximum stiffness of the material. Their study demonstrates that the optimum case for isotropic materials are auxetic,

have their poisson's ratio are not so small. They also studied four examples that are solved by using Isotropic Material Design.

1.3 Production of Materials with Negative Poisson's Ratio

The original structure of the material and the geometry that the material produced are the key two factors in producing auxetic materials. Auxetic materials have gained the negative Poisson's ratio throughout the macromolecule structure or macroscopic framework. Generally, auxetic materials are produced as foam, fibre or composite material. Still it is hard to produce auxetic polymers in macromolecular level. Auxetic foams are generally produced by volumetric pressing of conventional foams, or heating the polymers to the softening temperature and then cooling it at the same pressure.

L. Jiang, et al. produced auxetic composites throughout the processes of injection and foaming. First stainless steel and orthogonal auxetic reinforcement were placed in a metal template and then uniformly distributed polyurethane was added to the mixture by hand injection (Jiang, Gu, & Hu, 2016).

P. Subramani et. al produced auxetic materials by using vertical braiding machine, Figure 1.8. They used glass fibre reinforced composite rods to manufacture auxetic structures. Produced auxetic structures were tested physical and the results were compared with the numerical values (Subramani, Rana, Oliveira, Fangueiro, & Xavier, 2014).

Figure 1.8: Braiding machine that can be used to produce auxetic materials (Subramani et al., 2014).

Simplest way of producing an auxetic framework is using an unique geometry that makes the material behave as anti-conventional. The material can behave like auxetic material even if it has positive number of Poisson´s ratio. The material used in the production of the overall shape can be positive, but the way that material is produced makes the final shape auxetic. According to K.E. Evans and K. L. Anderson (K.E. Evans, 2000), the key to produce auxetic material is transcribing the process method that is already approved for large materials to the molecular level materials.

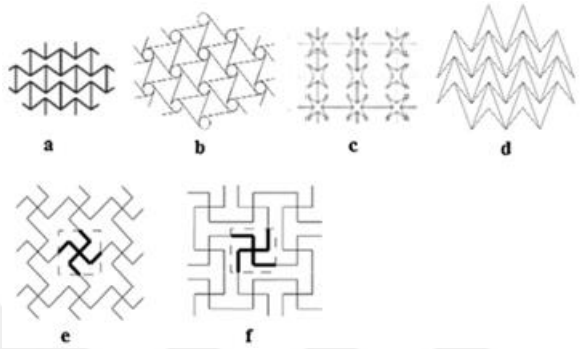

Figure 1.9: Different types of auxetic structures: a-) reentrant honeycomb, b-) chiral honeycomb, c-) star shaped honeycomb, d-) double arrow head honeycomb, e-) and f-) missing rib (Subramani et al., 2014).

Different kinds of structure shapes are given at Figure 1.9. Anti tetrachiral structure is also one of geometries that allow the material to shrink under compressive loadings and expand under tensile loadings. And it is one of the most used structures to create and test the abilities of the auxetic structures. This geometry can be seen in Figure 1.10 seperately.

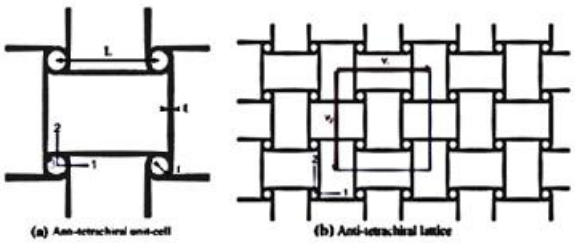

Figure 1.10: a-) A single cell of auxetic material b-) An image of auxetic frame. (Dirrenberger, Forest, & Jeulin, 2013)

Yanhong Ma et al. used anti tetrachiral framework in their experiments (Ma et al., 2013). The dimensions of the tested anti tetrachiral structure was 185 mm x 185 mm x 30 cm. Ligaments and cylinders have equal thickness of 2 mm. They also tried to

improve the material by filling the metal rubber particles into the cylindrical shapes, Figure 1.11. The results showed the potential for future experiments for anti tetrachiral structures with filled cylinders.

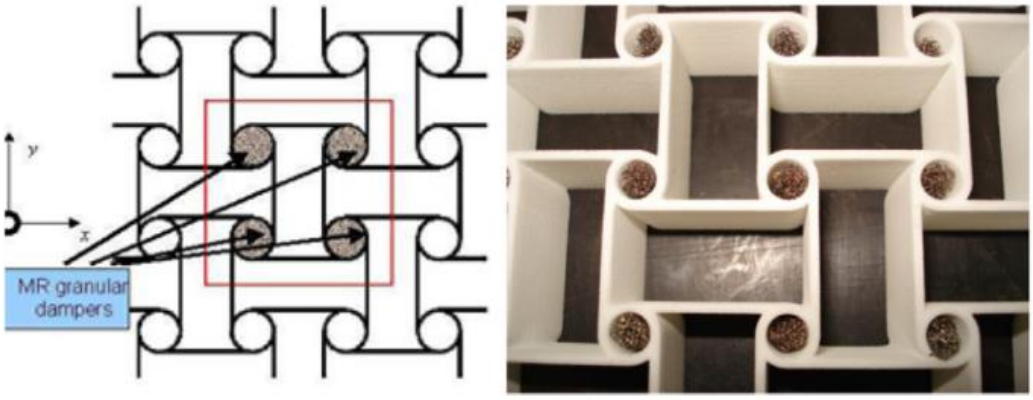

Figure 1.11: Anti tetrachiral framework with metal rubber particle filled cylinders (Ma et al., 2013).

Another production technique is used by R. F. Almgren, in order to design a 3D auxetic geometry starting from the 1D (Almgren, 1985). The main goal is to produce a material with a Poisson's ratio of -1. Reentrant type of auxetic geometry is selected and the optimum α value for the geometry is tried to find. The detailed reentrant type and the angle can be seen from the Figure 1.12.

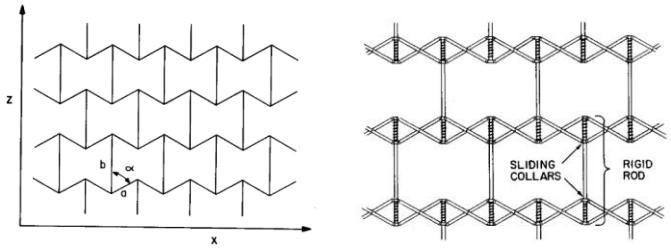

Figure 1.12: One dimensional auxetic structure(left), two dimensional auxetic structure(right) (Almgren, 1985).

The optimum value of α is found as 60°, and then the research moves to the second dimension. Passing from the first dimension to second dimension is through the shear stress and shear modulus, and the structure is extended in the x direction. The geometry must be now extended in y direction to get to the third dimension. And final shape of the geometry is given in the Figure 1.13.

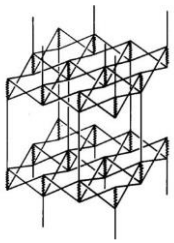

Figure 1.13: Final shape of the optimized 3D shape (Almgren, 1985).

Two different auxetic geometries are detailly inspected in this thesis. Reentrant geometry is compared with widely used honeycomb geometry by making numerical analyses. These analyses are proved to be true by creating the same analysis environment. Exact same situations with the numerical analyses are created to test the auxetic materials and to establish a relation between analyses and experiments. This thesis shows the importance of auxetic materials by comparing them with a conventional material. Also, a stiffer auxetic material is produced by using anti tetrachiral geometry. Both reentrant and anti tetrachiral structures are tested under edge crush test.

Mainly this thesis is organized under four sections. In Chapter 2, detailed explanation of the numerical analyses are given. Element and node information of the parts used in LS-Dyna software are introduced and their properties are explained. In Chapter 3, existing and new parts of the testing systems are described. Information about sandwich plates and experiment application processes are showed. As a final step, the comparison between numerical and experimental tests are compared in the Chapter 4.

2. NUMERICAL ANALYSIS

Main focus of this section is computer analyses. Information about numerical analyses process, performed analyses are shown in this section. Section starts with verification analysis to prove that created geometries show auxetic behaviour. After that, compression and impact analyses are explained elaborately.

Numerical analysis processes are performed in LS Dyna finite element program. LS Dyna is well known for many different usage areas, such as bird strike analysis, seatbelt and airbag analysis, failure analysis and metal forming. After the analyses, LS Dyna Prepost is employed for the visualization and the exploration of the results.

The specimens are prepared inside the LS Dyna Prepost interface. First of all, the created geometry must be tested. In order to test the newly created auxetic geometry, a simple compression test was performed in Section 2.1. After the verification of the negativeness of the auxetic geometry, a conventional geometry, honeycomb structure, was created. Auxetic and honeycomb geometries were compared for the abilities of durability, strength and absorbance of the load. Three main analyse types were handled for this task, namely in-plane compression loading, vertical plane blast loading and vertical plane impact loading.

2.1 Verification Analysis for Auxetic Geometry

At first, anti tetrachiral structure is studied in order to prove the negative Poisson´s ratio of created models. The model is a square with a dimensions 135 mm x 135 mm x 5 mm. Elastic Abs material is used for the auxetic core, since it is the material of most 3D printer and easy to produce complex structures. Abs+ material type is defined to the auxetic structure by using Mat_Elastic, whereas two plates are defined by using Mat_Rigid. The command Mat_Elastic is used for defining isotropic elastic material and it is commonly used for shell, beam and solid elements. Mat_Rigid is used to have a rigid shapes that does not buckle under applied loading. Main aim is to have a rigid body that can transfer the load to the specimen equally. The blue and green parts seen in Figure 2.1 are modelled by using Mat_Rigid. Load is applied on these two parts and

they are expected to distribute the load to the specimen equivalently. Applied loads are shown by F. Compression loading is obtained by compressing the two rigid plates together.

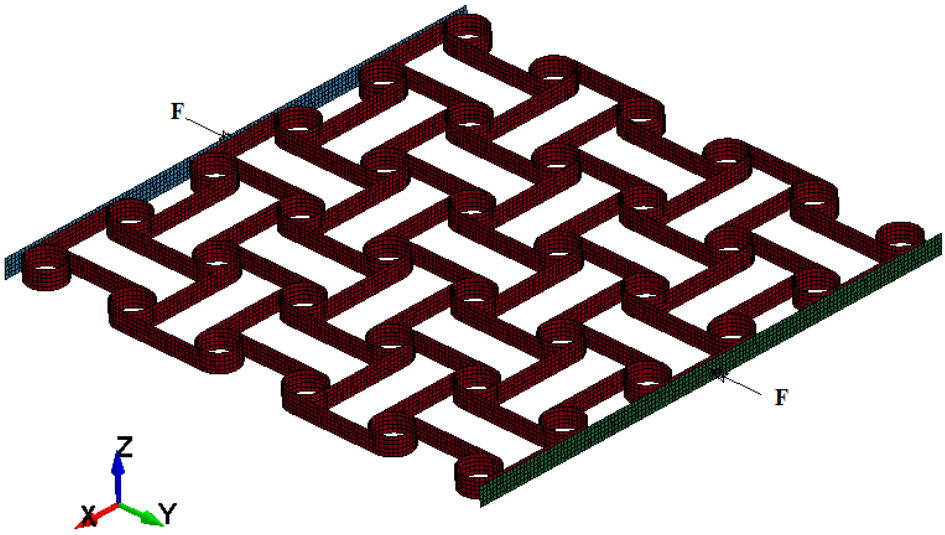

Figure 2.1: Auxetic specimen snalysis configuration for confirmation.

The material properties of the ABSplus (Acrylonitrile Butadiene Styrene plus) materials are given by the 3D printer producer as, densityρ= 1.04 g/cm^3, modulus of elasticity E=2200 MPa, and Poisson´s ratio of $\upsilon = 0.35$. Geometry effect was the main idea of the research, so only elastic material is used in the creation of the core part. The properties of steel that is used for the creation of particle and rigid plates are: densityρ= 7.85 g/cm^3, modulus of elasticityE=210 GPa, and Poisson´s ratio υ=0.30. Carbon fiber reinforced polymers are created by using deformable material type and they deformed during the analysis according to the failure criteria. CFRP have a density of $\rho = 1.65\ g/cm^3$, $E_{long} = 112\ GPa$, $E_{trans} = 112\ GPa$, $\upsilon = 0.35$, $X_T = 2070\ MPa$, $X_C = 1317\ MPa$, $Y_T = 61\ MPa$, $Y_C = 205\ MPa$. X_T is the longitudinal tensile strength, X_C is the longitudinal compressive strength, Y_C is the transverse tensile strength, and Y_C is the transverse compressive strength. CFRP is very weak when the load is applied on the transverse direction. CFRP layers are constructed perpendicularly in order to avoid transverse direction weakness.

The dimensions of the auxetic core are 135 mm x 135 mm and it has 5 mm thickness, and the dimensions of the honeycomb core are 135 mm x 130 mm and 5 mm thickness.

The small difference of the dimension of the cores is caused by the shape of the honeycomb cell. The dimensions of a hexagon are not equal in the x and y direction. This causes material to have unequal corner values. The dimensions of the honeycomb cell is changed later to have same dimensions as reentrant geometry.

Table 2.1: Element and node numbers of different parts.

	Anti tetrachiral Specimen	Honeycomb Specimen	Composite Layer
Type	Shell	Shell	Shell
Number of Elements	13260	18590	2808
Number of Nodes	15912	18364	2915

Cutting the honeycomb according to desired values does not yield trustworthy results, because the leftover part of the hexagon does not behave like hexagon and this changes the material properties of the honeycomb structure. Adequate values were selected for the corner dimensions, in order to have a reasonable comparison. A single cell of auxetic geometry has a 5 mm radius and 25 mm connection arm length. Each circle is 25 mm apart from other circles. And each line of a hexagon cell has a 10.4 mm dimension. The number of the elements and nodes are given in the Table 1 and the parts created according to this numbers are given at Figure 2.2.

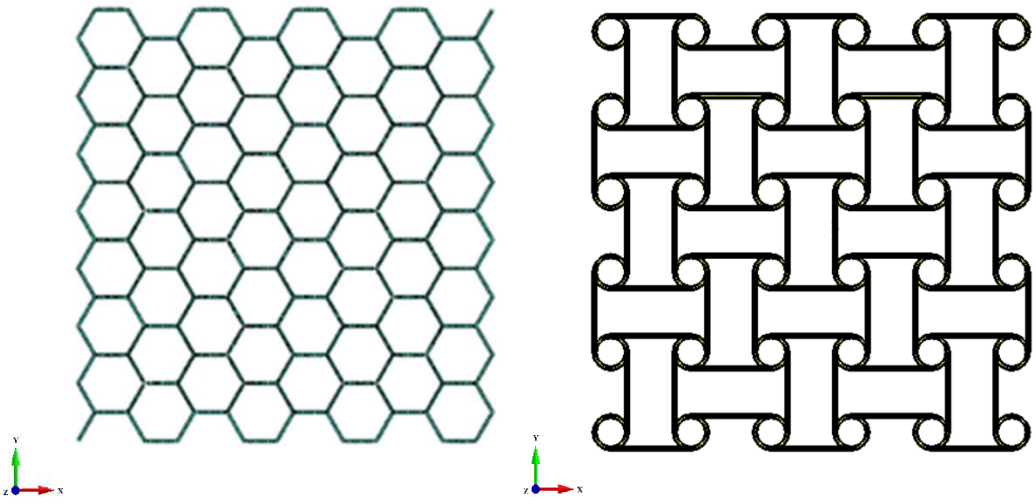

Figure 2.2: Shapes of the honeycomb (left) and auxetic (right) specimens.

After the cores were constructed properly, eight total layers were placed at the bottom and top of the core of the sandwich specimens. The layers were produced from the composite CFRP (Carbon Fiber Reinforced Polymer). The geometry is seen in the

Figure 2.3. In the figure, there are four layers above the core part and four layers below the core part. The layers were placed in either 0° or 90°. Layers that are closest to core part (Layer 4 and Layer 5) have 0° alignment for both lower and top part. The second closest layers (Layer 3 and Layer 6) have an alignment of 90°, the third closest layers (Layer 2 and Layer 7) have an alignment of 0°. And furthest layers (Layer 1 and Layer 8) have 90° alignment. Layers and their numbers can be seen clearly in Figure 2.3. Also, Table 2.1 shows the number of node and elements of each part. Layers are placed in this alignment in order to avoid the angle dependency. Also, layers have thickness value of 0.2 mm.

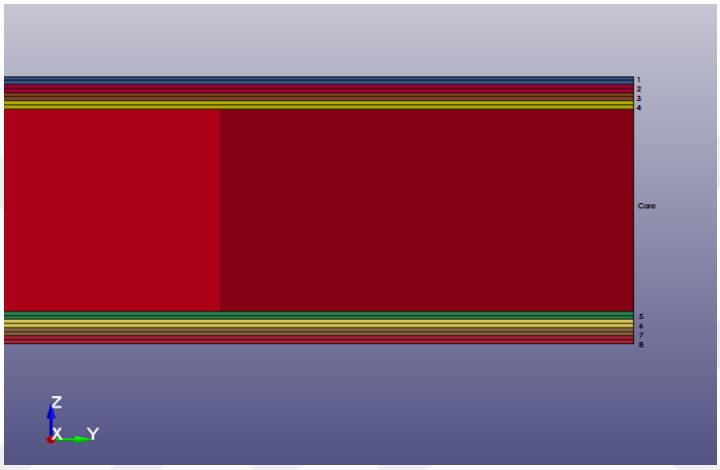

Figure 2.3: Core and the layers of the sandwich specimen.

The given specimen is analysed under compressive force to see the reaction of specimen. The analysis is done with the help of two rigid plates. The plates are placed at the sides of structure as seen in Figure 2.3. Plates are pushed to each other to compress the structure with 5 N load. The analysis was run for 5 milliseconds. The resulting displacement values in the x and y axes are given in the Figure 2.4.

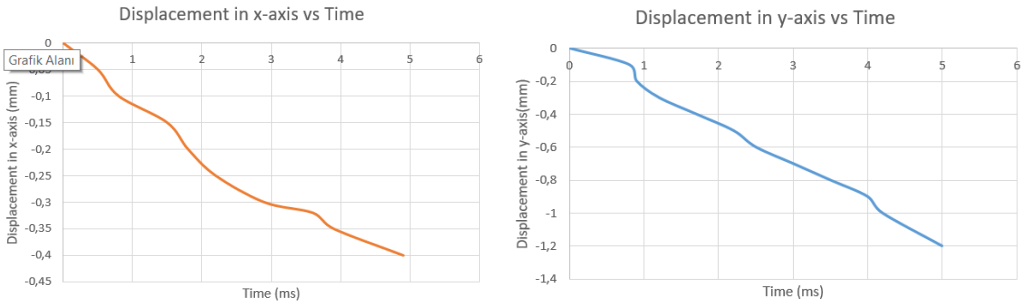

Figure 2.4: Displacement of the transverse direction (left) and longitudinal (right) vs time

Displacement is in mm, and the time is in milisecond. The displacement values are negative for both axes. The negativeness of the displacement values state that the length of the both sides are reduced. For conventional materials, if one direction has negative value of displacement then other direction is expected to have positive displacement value. However, displacement values for auxetic materials have the same sign for both directions. This analysis supports that this tested material has negative Poisson´s ratio.

Another verification analysis is done by using a different configuration. For this analysis, reentrant type auxetic specimen is selected. In this configuration, both plates and the main geometry are created as solid parts. Dimensions of the auxetic specimen is 195 mm*50 mm*135 mm, and the dimensions of the plate is 195 mm*3 mm*135 mm. Also auxetic specimen has 36774 elements and 70896 nodes, whereas each plate has 200 elements and 363 nodes. Mat_Rigid command is used for defining the material properties of a rigid steel to the plates. Also, Mat_Piecewise_Linear_Plasticity is used for ABSPlus material.

The reason of selecting different geometry type is to show that all of the geometries possesses negative Poisson's ratio. It is important to be sure that each specimen has negative Poisson's ratio. The geometric type of new specimen is given in the Figure 2.5. Left image shows the undeformed shape and the right image shows the final deformed shape.

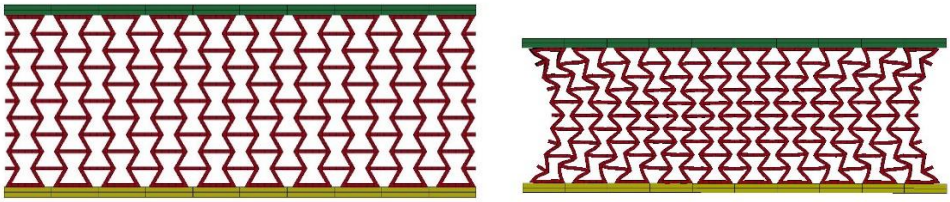

Figure 2.5: Undeformed (left) and deformed (right) shapes of reentrant type geometry.

Green and yellow parts are rigid plates, which are used to apply a compressive load of 50 kN to the specimen. The plates are pressed towards each other, in order to create compression on the auxetic geometry. The specimen, also called as reentrant type, behaves contradictive to the conventional material properties. Normally, it is expected to have an expansion in the transverse direction under compressive loading; however,

it shrinks not only on the longitudinal direction, but also on the transverse direction. Displacement values in x and y directions can be seen in the Figure 2.6.

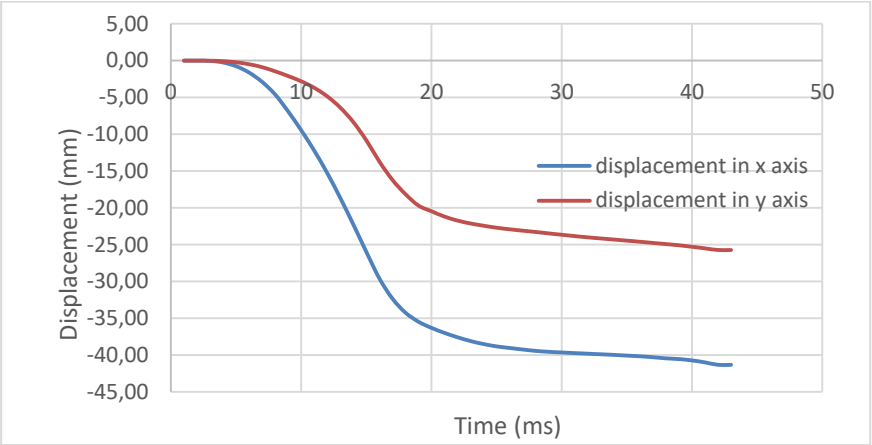

Figure 2.6: Displacement values of the specimen with reentrant geometry

The graphical result can be verified from the displacement value graph. Both directions have negative displacement values, implying that the specimen shrinks in every direction under a compression loading. This is the main requirement of being an Auxetic material. In addition, Poisson's ratio of the specimen can be calculated using the obtained displacement values. Note that, displacement values must be divided to the original length in that axis in order to obtain the strain value. Moreover, ratio of the strain values gives the Poisson's ratio. This ratio is calculated for each time step and given as a graph at the Figure 2.7.

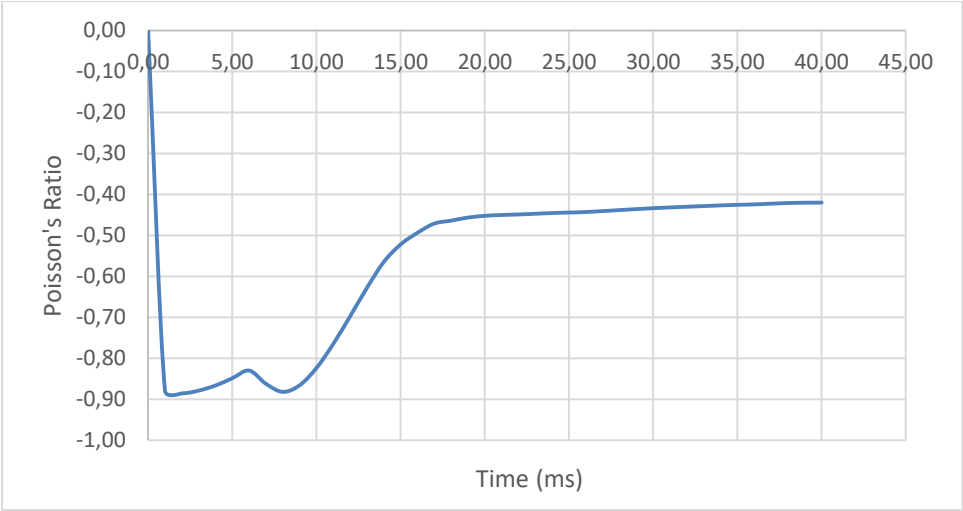

Figure 2.7: Calculated Poisson's Ratio of the specimen

The interesting part of this graph is the very beginning of analysis, where Poisson's ratio goes up to -0.89 and the slowly settles down to -0.42. The values of the Poisson's

ratio is in completely acceptable range. The peak at the beginning can be commented as an initial response of the material to the loading. After a few moment, roughly hundredth of a second, the ratio finds its ideal value.

2.2 Compression Analysis in Horizontal Plane

Horizontal plane has the best direction for examining the material properties of the specimens. As seen above, the auxetic behaviour of the anti tetrachiral geometry is proven. For this analysis, four different analyses are performed under four different loading conditions. Two rigid blocks are used to compress the specimens in y-direction, seen in Figure 2.8. Displacement values of each specimen and visual control are used to determine the effect of the geometry on the sandwich material.

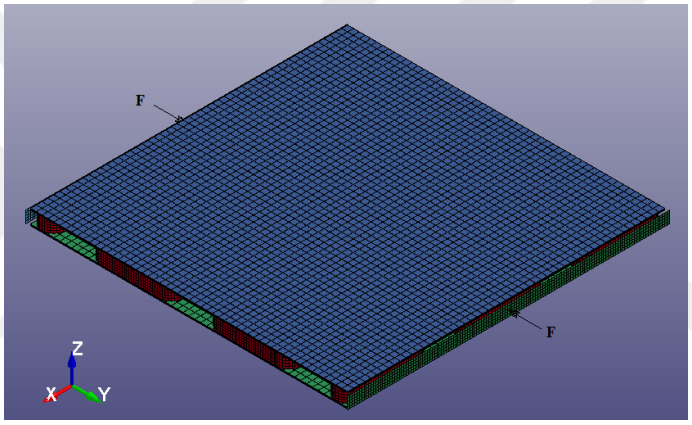

Figure 2.8: Sandwich structure with eight total composite layers and load application points

The rigid blocks are compressed through each other with forces 0.1 N, 1 N, 5 N and 25 N. The load is zero when the time is zero and it instantly reaches its top value. The unit loading curve can be seen at Figure 2.9. Appropriate scalar values are used to multiply and to get the desired loading value, i.e. 25 is used as a factor in the finite element program to get the desired load value. All of the loads are applied to the two points shown in the Figure 2.8. In the figure, the load is shown as a single load. However, the plates that loads are applied are rigid and move as a solid. Hence the sandwich structure can be compressed equally.

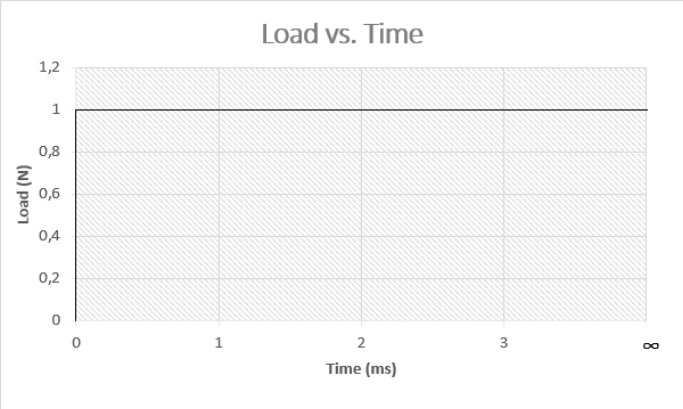

Figure 2.9: Standard loading curve that is used to define different loading cases.

Poisson´s ratios of the specimens were calculated from Equation 2.1. This is the general equation of Poisson´s ratio. Since most of the materials have positive Poisson's ratio, there is negative sign in front of the equation. dε is the ratio of extension of the material to the original length of the material in any direction.

$$\nu = -\frac{d\varepsilon_{transverse}}{d\varepsilon_{longitudinal}} = -\frac{\Delta L_{transverse}}{L_{transverse}} * \frac{L_{longitudinal}}{\Delta L_{longitudinal}} \tag{2.1}$$

Tetrachiral structure was designed as a square, so the lengths of both longitudinal axis and transverse axis are equal, $L_{longitudinal} = L_{transverse}$. The equation for calculating the Poisson´s ratio of tetrachiral shapes can be simplified to:

$$\nu = -\frac{\Delta L_{transverse}}{\Delta L_{longitudinal}} \tag{2.2}$$

But the situation is a bit different for the honeycomb structure. (Eq. 2.1) must be used for the calculations, as honeycomb structure is not a square shaped like tetrachiral structure. This difference comes from the shape of the honeycomb structure, as the lengths of the honeycomb cell in x and y axis are not equal to each other.

First of all, the Poisson´s ratio values of the tetra-chiral geometry is calculated according to (Eq. 2). The geometry had a Poisson´s ratio between 0 and -0.1 for the lowest loading condition of 0.1 N. It can be said that the loading is too easy for the specimen, it had very few impact on the specimen.

For the loadings of 1 N and 5 N, the specimen had an average Poisson´s ratio of -0.4. There is a peak value of -0.9 for both analyses. It is assumed to be occurred due to the

first stage of loading. The specimens are reacted too sudden to the loading, but the ratio became stable after a very short period of time.

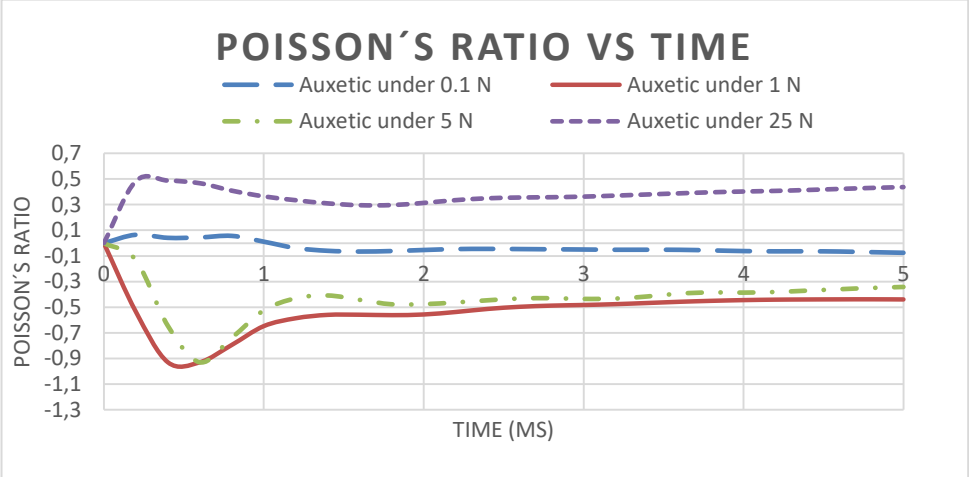

Figure 2.10: Poisson´s ratio calculations for the tetra-chiral structure under in-plane compression loading.

The strange part of the Figure 2.10 was the positive Poisson´s ratio of the tetrachiral shaped specimen under 25 N loading. It is assumed to occur due to relatively heavy loading. As the loading was too much for the specimen, it could not resist and the specific characteristic of the geometry was not maintained. The Poisson´s ratio in the stable region is very close to the Poisson´s ratio of the ABSplus material, which is 0.35. The auxetic geometry under 25 N loading collapsed inwards, and could not keep the geometrical properties. On the other hand, specimens under 1 and 5 N loading conditions behaved as they should, showing the auxetic behaviour.

2.3 Impact Analysis

The main idea of the impact test is to throw a particle to the specimen and investigate its behavior. The analysis is done in LS Dyna software by accelerating a particle with 10 mm radius. The sandwich plates are made of ABS+ core material and Aluminuim plates. Three different core shapes are used to make comparison; namely anti tetrachiral, reentrant, and honeycomb. Reentrant and honeycomb structures are produced in order to interperet with respect to each other; hence, they have exact same cell dimensions. However, anti tetrachiral structure is produced in order to have a structure as stiff as possible. At the same time, its thickness must be big enough to be printed from Infotron 3D printer.

A particle that is thrown at the specimens is created as a solid element and it has 875 elements and 976 nodes. The material properties of the particle is defined by Mat_Rigid, just to have an undeformable rigid element. The shape and the velocity of the sphere particle can be seen in Figure 2.11. All of the parts are created as a solid element.

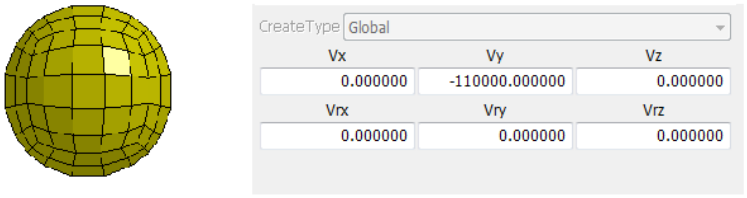

Figure 2.11: Solid sphere ball and defined velocity (110 m/s).

The velocity of the particle can be adjusted from the window seen in the Figure 2.11. Desired velocity values are given by Initial_Velocity command. The velocity of the particle that is used in the experimental setup is measured and then this value is used in the numerical analysis.

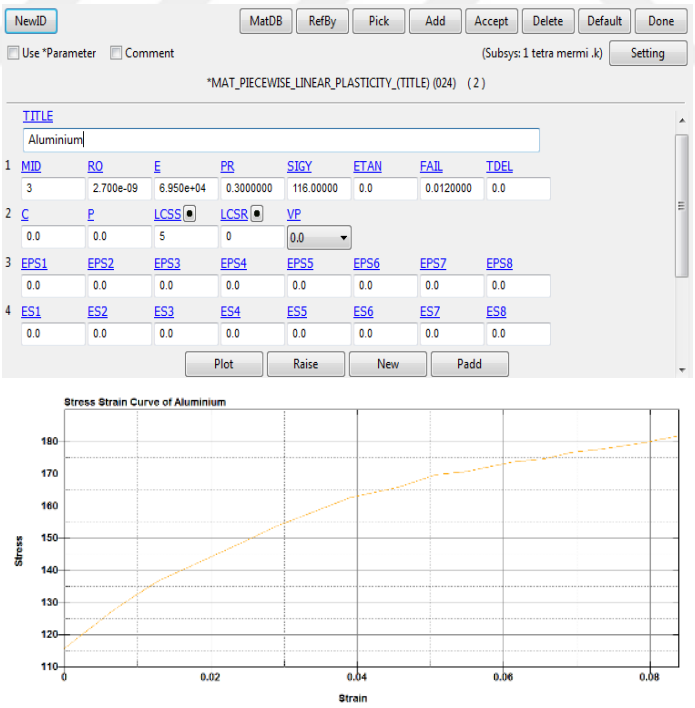

Figure 2.12: Material properties of Aluminium (above) and stress-strain curve of it (below).

After defining the sphere ball, material properties for core and outer layers are defined by using Mat_Piecewise_Linear_Plasticity. This material type allows structures to deform and even fail if a fail criterion is defined. Material properties are obtained from the coupon tests and detailed information will be given in the section 3.2. Coupon Tests. The screenshots of the material definitions that are taken from the finite element program can be seen in Figure 2.12 for Aluminuim, Figure 2.13 for ABS+ and Figure 2.14 for rigid steel.

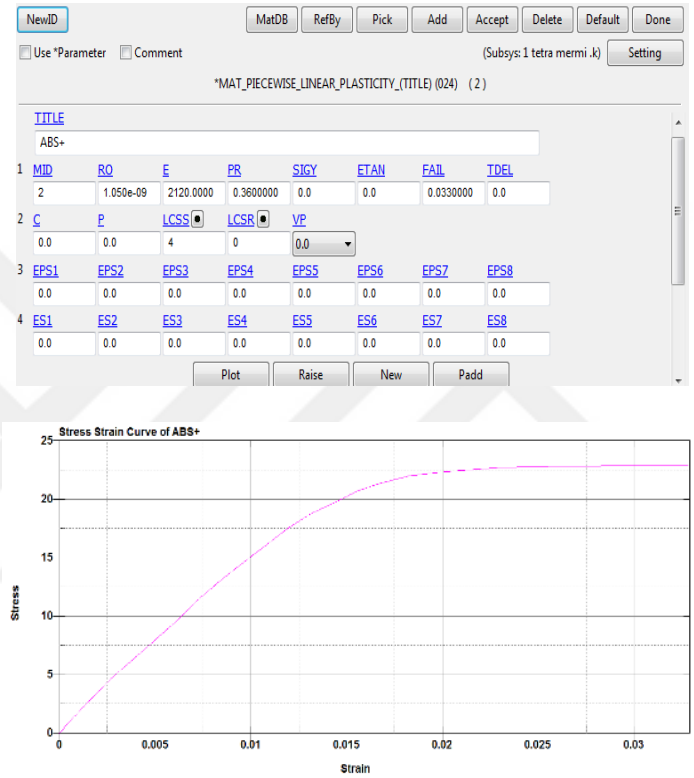

Figure 2.13: Material properties of ABS+ (above) and stress-strain curve of it (below).

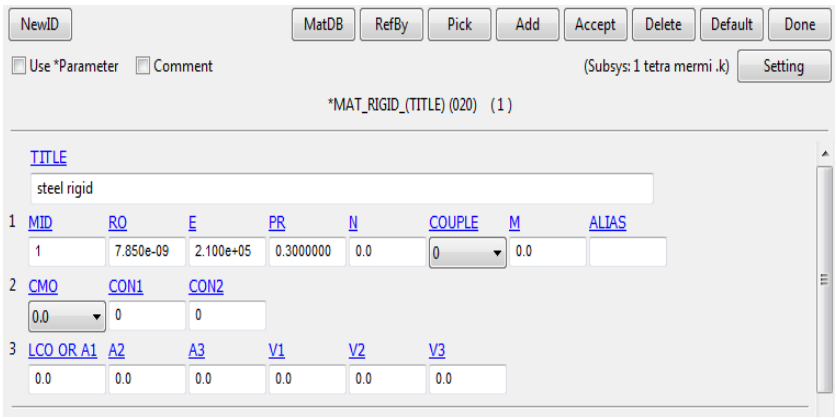

Figure 2.14: Material properties of rigid steel.

Actual values of the material properties are crucial for numerical and experimental analysis comparison. The material properties are obtained very carefully according to the ASTM standards, and the determination process is explained in the Section 3.2. Also, some important values of these properties are given as a table in the Table 2.2.

Table 2.2: Material properties used in the analysis.

	Aluminium	**ABS+**	**Rigid Steel**
Young‘s Modulus (Gpa)	69.5	2.12	210
Poisson‘s Ratio	0.3	0.36	0.3
Density (g/m3)	2.70	1.05	7.85

Next step after defining the material properties is defining the contacts between parts. After trying different types of contact, Automatic_Surface_To_Surface is seen to work best for this application. There are four parts in each of the analysis (two layers, one core, and one particle). The contact is defined between each two parts in order to see the results better. The main window of the contact section can be seen in Figure 2.15.

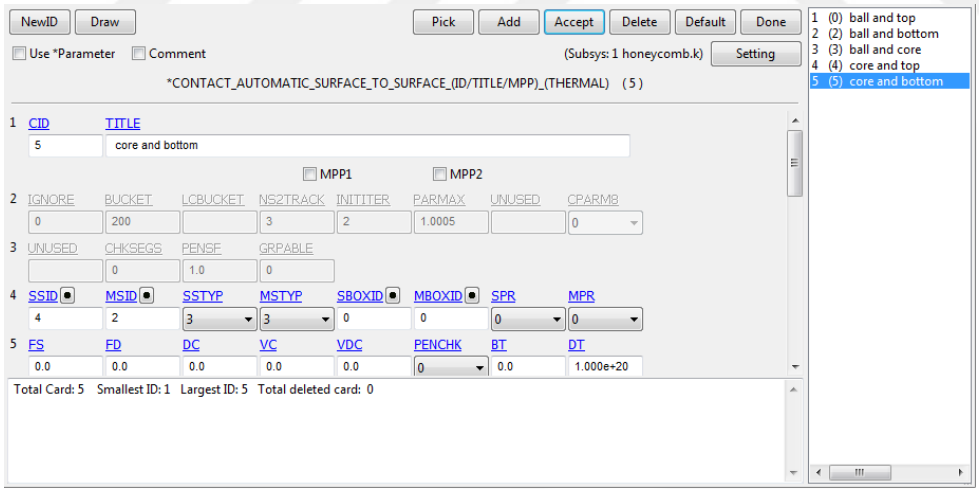

Figure 2.15: Contacts between each part.

As a next step, the boundary conditions must be defined. In the experimental setup the specimen is held to the testing frame by the clamps from all its edges. Accordingly, the numerical analysis must be matched up to this configuration. All four edges of the specimens are set to fix by boundary conditions, in order to obtain the same testing environment. This boundary conditions can be seen in Figure 2.16.

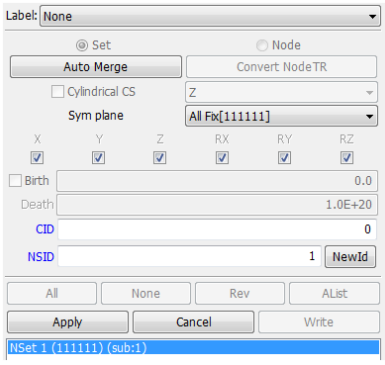

Figure 2.16: Boundary conditions of all four edges of a sandwich structure.

Boundary conditions are defined with an “all fix” command under Boundary_Spcset section, implying zero degree of freedom for force and moment components of any axis. As a final step, termination time is defined under Control_Termination section. Since the impact effects occur very rapidly, 40 miliseconds are selected as a closure time value. And time step value is defined under Database_Binary_D3plot section as 1 milisecond. In Figure 2.17, termination properties for the analysis can be seen.

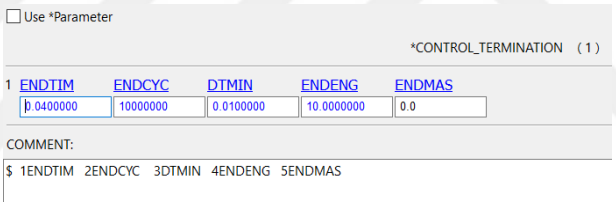

Figure 2.17: Termination properties of the analysis

These numerical analysis properties are essential for any finite element program and must be well defined before analysis starts. Some of the possible problems that can be encountered in Ls Dyna are negative volume error and dimension inconsistencies. Dimension inconsistencies are easy to overcome, but requires a bit more detailed inquiry. On the other hand, negative volume error is harder to overcome. It occurs when working with solid materials, and these solid materials are subjected to significant deformation. Material properties and contact types should be looked over again, and possible interlacings of the parts should be controlled.

2.3.1 Impact analysis for honeycomb geometry

Honeycomb geometry is one of the most common geometry that is used in the sandwich structures. And it is selected as a conventional shape for the analyse. A single

edge of the honeycomb cell is 5.774 mm. The main geometry can be seen in Figure 2.18.

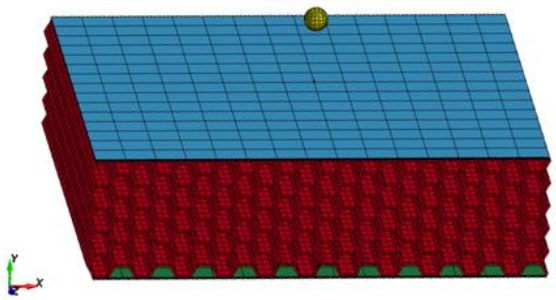

Figure 2.18: Impact analysis configuration of the honeycomb shape.

There are four parts in this analysis. The core part is covered with two layers of aluminium to create sandwich structure. And a particle is used to create the impact loading effect.

Honeycomb core has 38883 elements and 73358 nodes, where each layer of Aluminium has 300 elements and 484 nodes. The particle's element and node numbers are given in the section above. All four edges in the x-z dimension is fixed and all of the parts are solid material. Speed of the particle is 110 m/s in the negative y direction.

The analysis is run for 40 miliseconds with a time step of 1 milisecond. And the result of the analysis is given in the Figure 2.19.

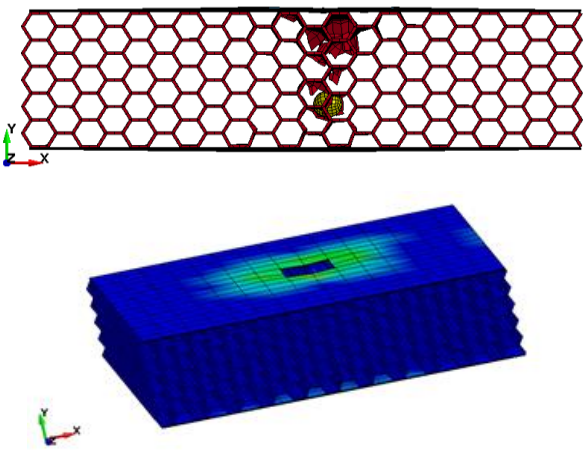

Figure 2.19: Side (above) and perspective (below) views of the honeycomb geometry.

Max stress value occurred in the analysis is 78.45 MPa, and the movement distance of the particle inside the honeycomb core is 34.33 mm. Also, the stress value change with the time is given in the Figure 2.20.

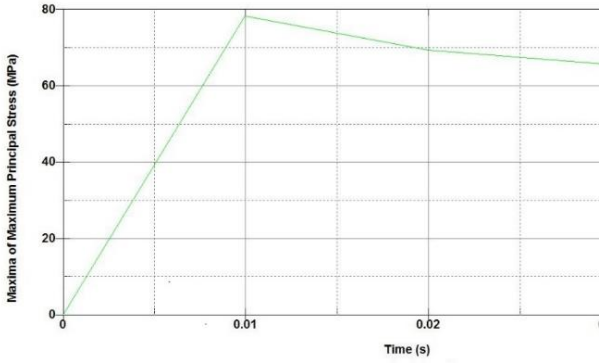

Figure 2.20: Maximum stress values occured at honeycomb analysis.

The stress values and the total distances travelled by the particle inside the core parts are going to be discussed further in the following sections.

2.3.2 Impact analysis for reentrant geometry

Reentrant geometry is the first geometry that will be used in the analysis. Since it is a geometry that is derived from the hexagonal shape, it is a wise decision to make a comparison between hexagonal (honeycomb) and reentrant geometries. For this manner, the unit dimensions of the reentrant geometry is the same as the hexagonal dimensions. Therefore, a single cell of the reentrant structure is comprised of 5.774 mm short arm and 11.112 mm long arm. The angle between each short and long arm is 60 degrees. Reentrant geometry and the analysis configuration can be seen in Figure 2.21.

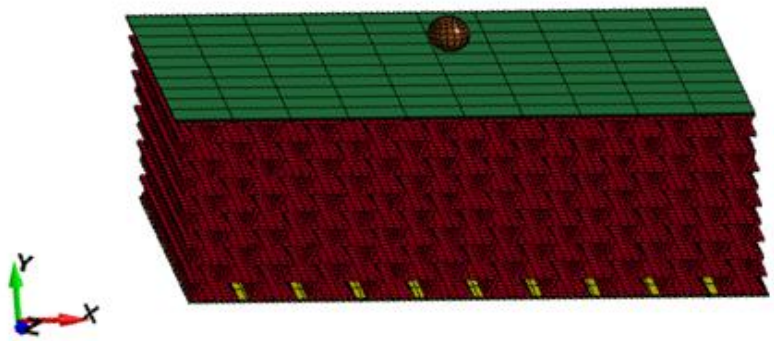

Figure 2.21: Impact analysis configuration of the reentrant shape.

All of the properties and the setting are the same with the honeycomb analysis. Only difference is the core part is modified to a reentrant structure, in order to see the auxetic effects. The analysis time and time step is not changed, and the final form of the analysis is given in the Figure 2.22.

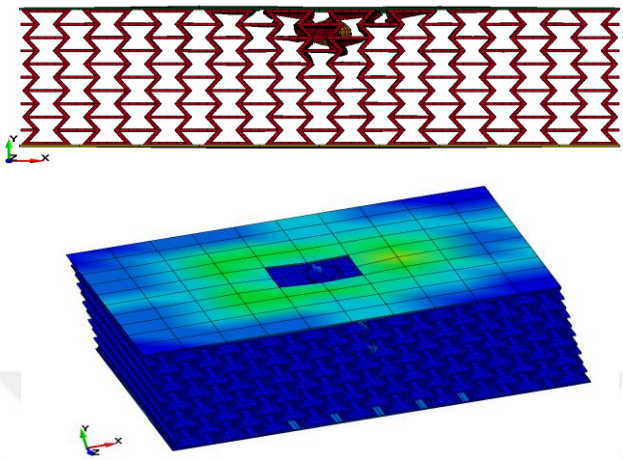

Figure 2.22: Side (above) and perspective (below) views of the reentrant geometry.

Maximum stress value that occurred in the reentrant cored analysis is 47.15 MPa and it occurred during the beginning phase and remained nearly constant. Max stress can be seen in the Figure 2.22.

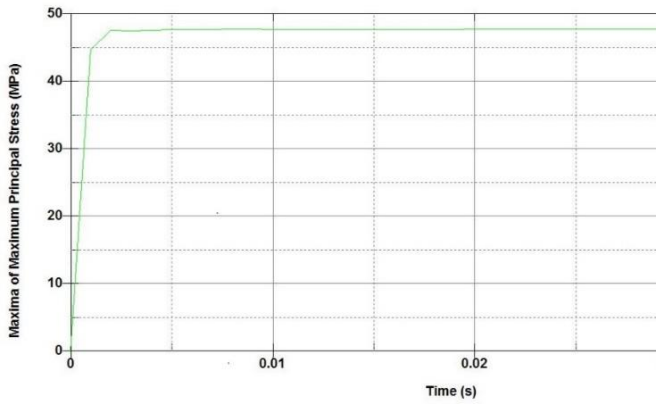

Figure 2.23: Maximum stress values occured at reentrant analysis.

This maximum stress value is smaller than the value encountered in the honeycomb analysis. Also, the particle moved 13.2 mm inside the reentrant core, where it travelled 34.33 mm inside the honeycomb core. These two comparisons show that the reentrant geometry behaved better under impact loading. Since the auxetic behaviour is proved for the exact same geometry, it easily be said that auxetic materials behaved better under impact loading.

2.3.3 Impact analysis for anti tetrachiral geometry

Anti tetrachiral geometry is created by pushing the limits of the 3D printer. Hence it is much denser than both honeycomb and reentrant structures. Considering the denseness and the cell dimensions, it will not be fair to compare anti tetrachiral geometry with other two geometries. Hence, main reason of this part is to see the effect of denser geometry type, and comparison between numerical analysis and experimental test. Main configuration of the anti tetrachiral geometry is given in the Figure 2.24.

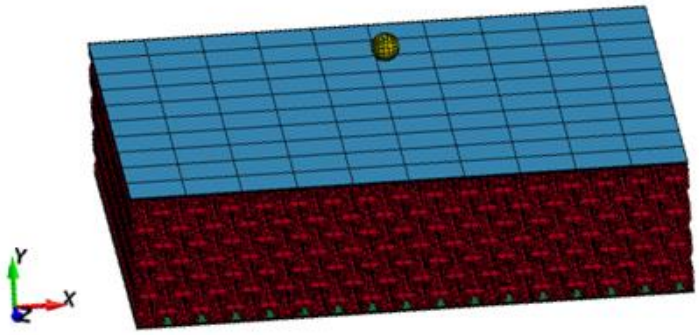

Figure 2.24: Impact analysis configuration of the honeycomb shape.

The only differences of the anaylsis are the unit cell dimensions and the velocity of the particle. Since the particle had hard times moving through the auxetic reentrant geometry, the required velocity to penetrate to the anti tetrachiral geometry is predicted to bemuch higher. For this manner, the velocity of the particle is adjusted to 120 m/s, which is the max velocity value that can be obtained at the experimental test. However, this velocity was also not enough to impale through. The main reason of this is the anti tetrachiral geometry was initially designed to withstand velocity values up to 250 m/s. but the oppurtinities was limited and the velocity value had to be restricted to 120 m/s. The cell shape and the layers can be seen in the Figure 2.25.

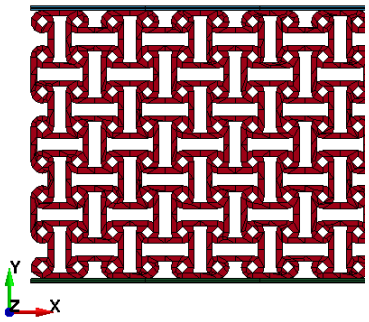

Figure 2.25: Anti tetrachiral geometry.

The differences of the Figure 2.25 from the Figure 2.1 are the cell dimensions and the layers. Composite layers are used in the Section 2.1, however, the layers are changed to aluminium and the number of the layers are decreased from four to one. This one single layer of Aluminium has 0.75 mm thickness. These Aluminium layers have 300 elements and 484 nodes, where anti tetrachiral core has 107100 elements and 147001 nodes. The diameter of each circle in the anti tetrachiral structure is 2 mm, and the ligaments connecting the circles are 6.125 mm. Also, each both circles and ligaments have 1 mm thickness. The result of the analysis can be seen in Figure 2.26.

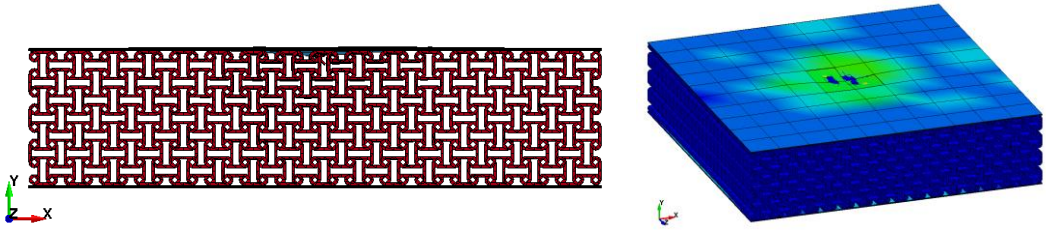

Figure 2.26: Side and perspective view of the anti tetrachiral geometry.

120 m/s is not high enough to penetrate the core part. It only pierced the aluminium layer, and gave a little deformation on the surface of the anti tetrachiral core. And the movement of the particle is measured as 2.7 mm. the maximum stress distrubition of the anti tetrachiral core can be seen in Figure 2.27.

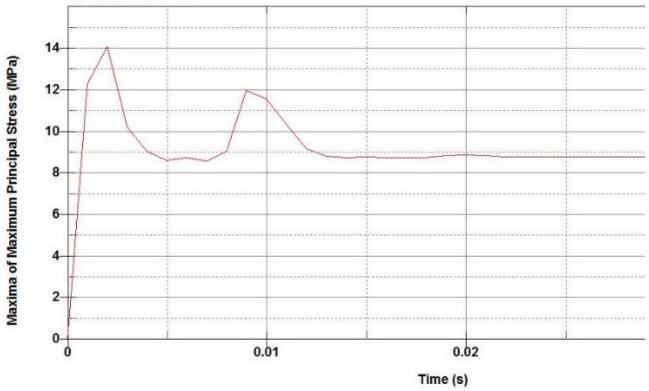

Figure 2.27: Maximum stress values occured at anti tetrachiral core.

Maximum stress value is measured as 14 MPa for anti tetrachiral core, a value much smaller from both reentrant and honeycomb geometries. Also, the visual results approve this value.

The results of the analyses came to exist as predicted. The stiffest structure is the sandwich antitetrachiral core, as the cell dimensions are much smaller and the cells are

much closer to each other. The compact shape of the anti tetrachiral core allowed it to stand stronger against the impact loading. Nevertheless, the comparison between reentrant and honeycomb structures are more meaningful as they have same unit cell dimension and same cell intensity.

Penetration distance is a weighty matter for impact loading. The distance can be lethal for critical cases, and keeping the penetration distance as small as possible is the key topic for impact loading researches. The particle travelled more distance in the honeycomb core, than the reentrant core. In addition, the maximum stress value occurred during the impact loading was higher for the honeycomb case. Another important topic for impact loading is having smaller stress value, as to keep the material under a certain region. Reentrant geometry had smaller max stress value too. This also shows the advantage of auxetic materials. In the light of the facts mentioned, it is safe to say that using auxetic materials is better than the conventional materials.

First analysis of this section was done to prove that reentrant and anti tetrachiral structures have negative Poisson's Ratio. After this demonstration, impact loading analysis was done on reentrant, anti tetrachiral and honeycomb structures. A comparison between reentrant and honeycomb was made as they have same unit cell dimensions. Auxetic structure was shown to have better impact resistance than conventional structure. Also, compression analysis was done on different anti tetrachiral structure with different load values. After this analyses, the cell dimensions of the anti tetrachiral structure was enhanced. Enchanced anti tetrachiral structure gave better results in the impact analyses. As anti tetrachiral structure had much denser geometry, it was kept out of the comparison between reentrant and honeycomb structures. However, it was a good example of a stiff auxetic material. At the next section, these structures are procuded from 3D printer and tested at the same conditions.

3. EXPERIMENTAL ANALYSIS

Existing tools are introduced in this chapter. Also new tools are designed and produced according to the experiment needs. The process of material properties' determination is explained in this chapter. After that, impact tests are performed on sandwich structures that are produced from reentrant and anti tetrachiral cores. Edge crush test is also performed on small pieces of reentrant and anti tetrachiral structures. Experiment results are compared with numerical results.

3.1 Brief Introduction to Experimental Tools

Before moving to the experimental tests, it is important to know the specifications of them. This allows future researches to create the same experiment conditions. In this manner, the characteristics and the operation ranges of the equipments that are used during the research are introduced in this section.

3.1.1 Infotron dimension elite

Complex and complicated geometries were hard to test due to the difficulty of production process. However, improved technology allows scientists to create complex geometries more easily. In this manner 3D printers can be considered as a milestone in the manufacturing process. Main shapes of this research were produced by using Dimension Elite 3D printer. The printer is shown at Figure 3.1.

Dimension Elite 3D printer works best at room conditions with 15-30°C and 30% - 70% relative humidity. These conditions should be kept constant during the manufacturing process. The machine has two cartridges, one for the model (ABSplus) and one for the support (Soluble Support Technology). A special solution is used to separate the support material from the main shape after manufacturing process. The machine has a manufacturing capability in the sizes 203 x 203 x 305 mm. Minimum layer thickness can be adjusted from the user interface as 0.178 mm or 0.254 mm.

Figure 3.1: Image of Dimension Elite-Infotron®.

3.1.2 MTS 322 test frame

Properties of the used materials are need to be determined before the experimental tests. By this way the material properties used in computer models will be real values and the results of the experimental and mathematical models will be similar. It is important to obtain the material properties in order to obtain better finite element results. Material properties are determined by using MTS 322 Test Frame machine. The machine has the capability to apply 100 kN compression or tensile forces. Also 25 kN side force can be applied by this machine. The MTS machine is shown at Figure 3.2.

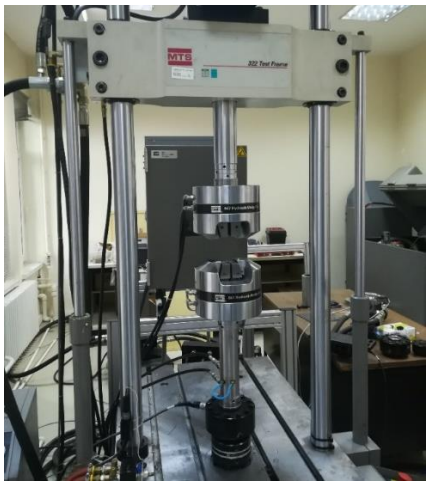

Figure 3.2: Image of MTS 322 test frame.

Also extensometer was used to determine the Poisson's ratio of the materials. Extensometer is also product of the MTS Company and the model number is 634.12F-24. It has 350 Ω normal bridge resistance, 25 mm gage length, 35.051 mV at Overtravel Stop(+ output), -8.370 at Overtravel Stop (- output), and 6.000 V output's excitation voltage. Also, there is an environmental chamber of the testing machine that can be used to create an environment with a temperature range from -110°C to 310°C. Additional part of the MTS machine, extensometer, is shown in the Figure 3.3.

Figure 3.3: Image of the extensometer.

3.1.3 Strain gauges

Strain gauges are attached to the specimens that are going to be used in the process of material properties determination. The properties of the materials were determined by the help of the voltage values produced by the strain gauges. The strain gauges are shown in the Figure 3.4.

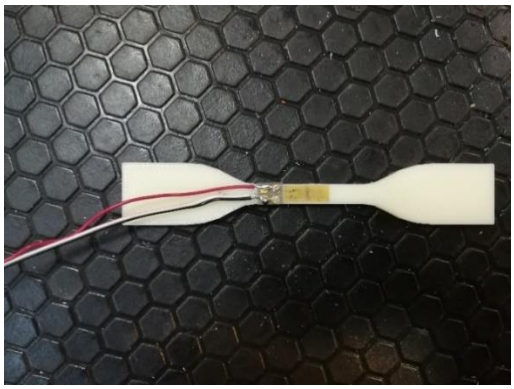

Figure 3.4: A specimen with attached strain gauge.

Strain gauges used in this research are products of Tokyo Sokki Kenkyujo Co. Ltd.. Their type number is GFCA-3-50. They have 3 mm gauge length, 120 ± 0.5 Ω gauge resistance, 1.1% tranverse sensitivity, and $50*10^{-6}$ /°C temperature compensation. Also, both of the gauge factor values are 2.09 ±1%. The recommended test condition is 23°C and 50% relative humidity.

3.1.4 Main testing device

Special device was designed to perform the impact experiments. The device can throw particles up to 120 m/s velocity value. Device was covered with a metal frame as a safety precaution. Moving plates inside the testing system allows us to move the specimen freely in both directions, and enables us to have impact force at different points on the specimen. Specially crafted testing device is shown in Figure 3.5. The cap can be opened for cleaning and maintanence, but it is preferred closed as a safety precaution.

Figure 3.5: Inside (left) and outside (right) of the testing device.

System has three different stages. First part is the compression tank. This tank has pressure value of 100 kPa. The pressured air is then transferred to the second phase. In this stage, smaller pressure tank is used to store the pressured air, shown in Figure 3.6. This tank can store air with 40 kPa pressure. Generally, 18 kPa is enough to generate 100 m/s speed values. The operating condition of the pressure tank improved with the recent maintanences, and the maximum of 120 m/s velocity obtained with 25 kPa pressure value. However, using air with a pressure value higher than 25 kPa may cause incidents during the experiment for this configuration.

Figure 3.6: Pressure tank.

After having enough pressured air, the pressured air is released through the small barrel, this barrel can be seen in the Figure 3.6. This triggers the small particle placed inside of the barrel. The particle is accelerated to desired speed at the end of the process. The barrel has 25 mm inner diameter and 35 mm outer diameter. The thrown particle and its holder can be seen in Figure 3.7. Also, their technical drawings are given for better understanding.

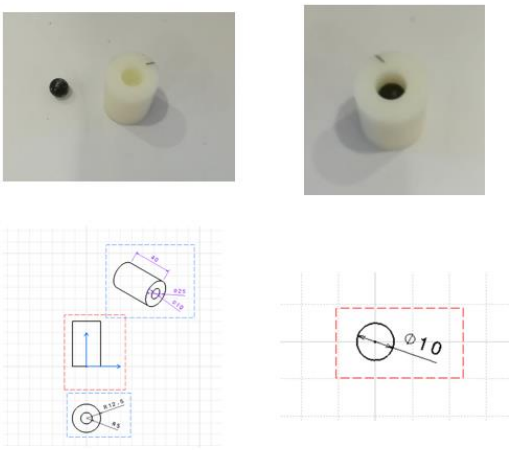

Figure 3.7: Thrown particle, its holder and their technical drawings.

The speed of the thrown particles are gauged by commercially available speedometer produced by the company MagnetoSpeed. This speedometer has an operating speed range from 91 to 2134 m/s, and it is more than enough to measure the speed values occurring during the experiments. The speedometer is fixed inside of the case, so that it measures the speed but not disturbs the particles flying through. Also, the image of the speedometer is given in the Figure 3.8.

Figure 3.8: Magneto speedometer.

Besides, some new parts had to be designed for inner part of the testing system. Firstly, the frames were needed to hold the specimens at the desired place. For this necessity, a frame designed was made. The frame was drawn in the Catia CAD software. Also, it was produced from a private company. The technical drawing and the produced frame can be seen in the Figure 3.9.

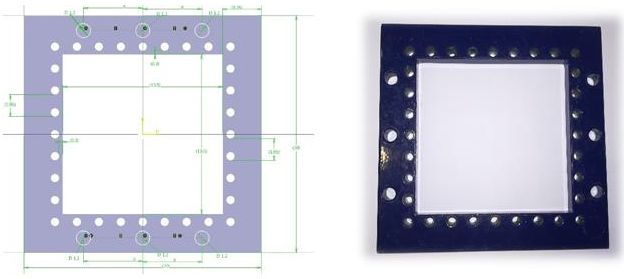

Figure 3.9: Design and produced form of the frames.

Moving parts of the testing device are not enough to hold heavy plates. As a last step, bench clamps were designed to constrain the specimens to the frames. By this way, the model could be connected to the free moving parts of the testing mechanism. Technical drawings were drawn on Catia software according to the requirements and clamps are produced from a private company. The detailed drawing of the bench clamp and the produced form of it is given in the Figure 3.10.

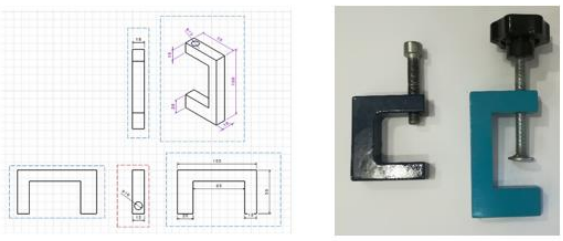

Figure 3.10: Bench clamp design.

3.2 Coupon Tests

Coupon tests are the crucial examination of the material properties, if the researcher wants to correlate between experimental and numerical analyses. It is very important to use the exact values in the numerical analyses to see better results. In this manner, coupon tests for ABS+ and Aluminium materials were performed according to ASTM standarts. Prepared samples can be seen in the Figure 3.11.

Figure 3.11: Prepared samples for coupon testing (ABS+ and Aluminium).

Coupon tests are done for multiple specimens and then the mean value is calculated from the obtained results. In the Figure 3.12, the analyses results for ABS+ material can be seen for four different specimens. Four different specimen are used to be sure that each specimen has the same properties. Then mean value of the specimens are used in the analyses. Same calculations are also done for aluminium and found values are entered to the LS-Dyna software.

Obtained results are also compared with the values produced from the ABS+ manufacturer and the results are validated before entering to the numerical analyses.

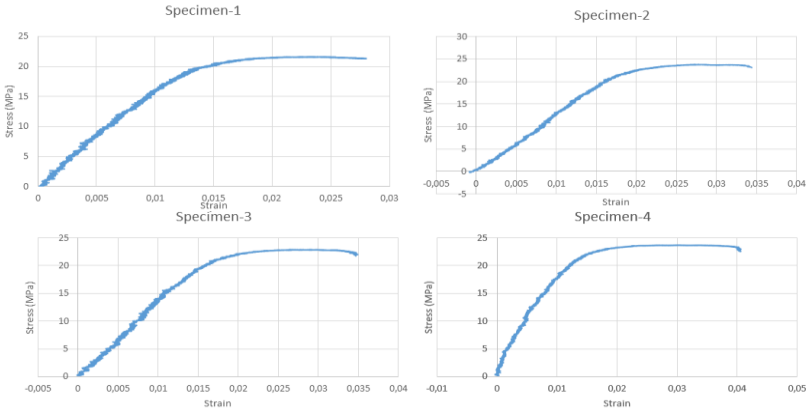

Figure 3.12: Coupon tests for ABS+ materials.

3.3 Impact Tests

Impact test is done by throwing a particle to the specimen and the behaviour of the specimen is analysed. Main reason of the impact test is to see the materials reaction against sudden loading, Thoughness and the response of the material are fundamental points on impact test.

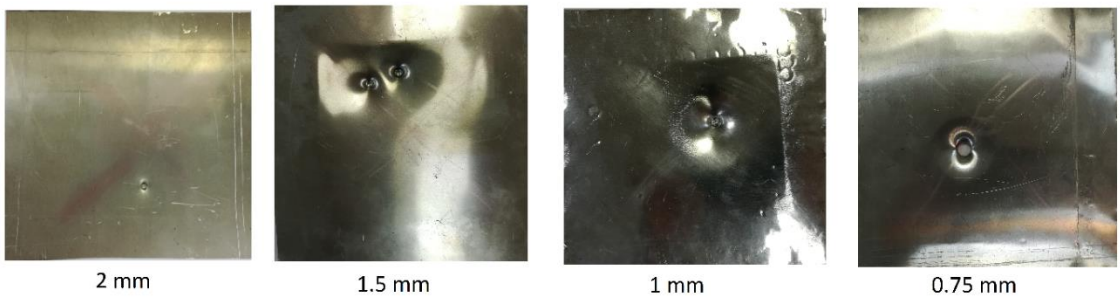

Figure 3.13: Trial shots to determine the suitable thickness value.

The major desire is to stop the particle inside the sandwich structure. In order to do that a velocity must be selected just enough to pass through the front layer of sandwich but slow enough to stop before reaching the bottom layer. By this way, the particle is going to be stopped by the core part. And the effect of the geometry of the core part can be seen better. Hence, the thickness of the aluminium plates must be selected properly. First, some numerical analyses are made in order to see the responses of different thickness values. After getting some information about the required thickness of aluminium, experimental tests are performed. Trial shots can be seen in Figure 3.13. First, an aluminium with 2 mm thickness is tested. 2 mm was too thick for particle to pierce the layer. Thus, the thickness is reduced to 1.5 mm, 1 mm, and finally 0.75 mm. The particle could pierce aluminium layers with a thickness lower than 1 mm. A choice between 1 mm and 0.75 mm must be done, before starting the experiment. Since the desired situation is having the particle travelled inside the sandwich plate, 0.75 mm is selected as a thickness value of the aluminium layers. The trial shots can be seen in the Figure 3.13.

Due to the financial issues, only auxetic materials are tested physically. Reentrant and anti tetrachiral geometries are produced from 3D printer with the exact same dimensions as used in the numerical analyses. Then they are fabricated into sandwich plates with aluminium plates, seen in Figure 3.14. The plates are then fixed to the testing device with the help of frames and bench clamps.

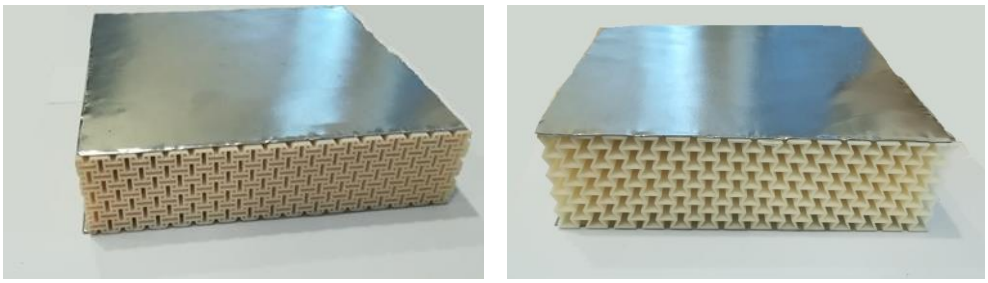

Figure 3.14: Sandwich plates with anti tetrachiral core (left) and reentrant core (right).

The limitations of the experiment are maximum compressed air value in the compression tank and size restrictions of the nozzle. Due to these restrictions a particle with maximum 10 mm radius can be accelerated up to 120 m/s.

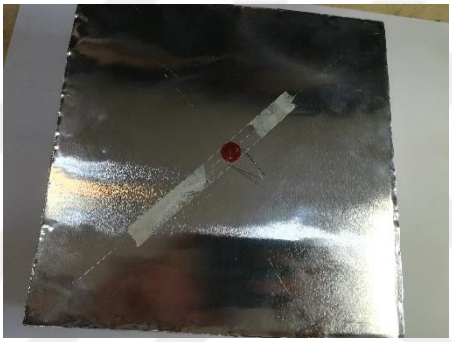

Figure 3.15: Strain gauge attachment process.

In order to measure data from the specimens, strain gauges are used. First, the surface of the specimen is well cleaned with isopropyl alcohol. Having smooth and clean surface is by far the most important thing in strain gauge application. Then the place of the gauge is adjusted with the help of a tape, seen in Figure 3.15. The strain gauge is glued with commercial super glue after the final position is found. During the bonding process pressure is applied with a finger for 70 to 80 seconds. Since the strain gauge does not have cables attached to itself, cables are soldered to the terminals with soldering iron. Two sets of cables are used, as this is a cross type strain gauge. Each specimen has three different strain gauges; two of them at the back and one of them at the front surface.

The specimen is almost completely prepared to test after attaching the strain gauge. As a final step the specimen must be placed to the testing frame with an adequate equipment. In Figure 3.16, clamped specimen can be seen. The specimen is ready for impact experiment.

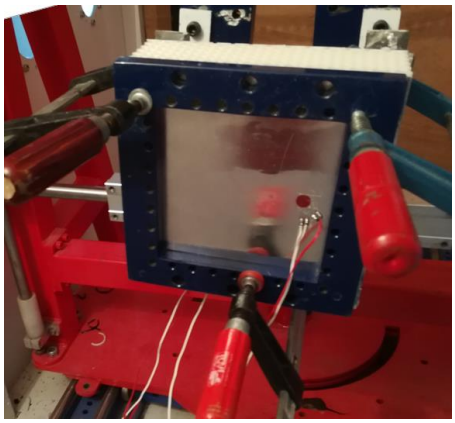

Figure 3.16: Clamped specimen.

Final results of the specimens are seen to be just predicted. In Figure 3.17, final results of the impact test are seen. Note that the particle is swerved a little bit from the middle point. This is caused by the low precision of the nozzle. But the impact point is not far away from the middle point, and causes not too much difference. Also the numerical analysis can be adjusted according to the final impact point of the particle.

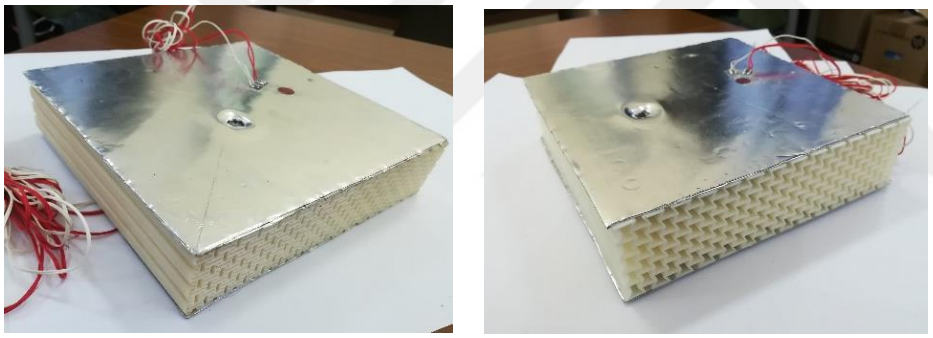

Figure 3.17: Results of the impact test for anti tetrachiral (left) and reentrant (right).

The particle moved inside of the reentrant core 12.5 mm, where it travelled only 2.7 mm inside of the anti tetrachiral core. The difference between two cores are originated from the denseness of the anti tetrachiral core. It is much denser than the reentrant core. However, this is not a problem since the reentrant core was produced to be compared with honeycomb core. Detailed comments about experimental results are made in Section 3.5. Numerical analyses of the same geometries are also compared in that section.

3.4 Edge Crush Tests

Edge crush test is important to see the specimen's crush resistance. Also the most crucial expectation of this test is to see the effect of gathering. Auxetic materials are

expected to gather around when a load applied to them. This phenomena is explained in the Section 1, with the help of indentation resistance. The same effect of the auxetic material is awaited in this experiment. One reentrant and one anti tetrachiral specimen are prepared for edge crush test. They both have 4 mm length and 4 mm width and 5 mm thickness.

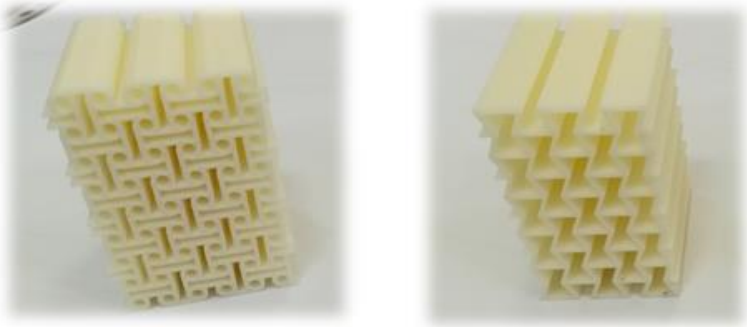

Figure 3.18: Specimens for edge crush test.

The experiment is done at the MTS that is introduced previously. Plates are moved 2 mm per minute as stated in the standards. Since the machine does not provide a load application center, this point must be found by hand. A systematic approach is made in order to find this point. The plates are precisely marked for the center point and the specimen is placed inside of the marks.

Photo of the specimen is taken at the certain time intervals for visual recording. Visual inspection is as important as data analysis, and it yields valuable information.

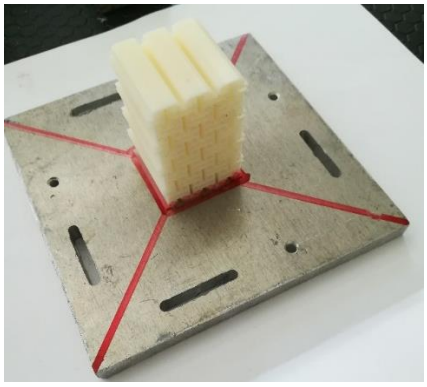

Figure 3.19: Centering the specimen.

It is curial to apply the load at the very middle of the specimen to prevent distortions. Plates are marked in order to find the middle point. After adjusting the middle point, the edge crush test is started. Steps of the experiment is given in the Figure 3.20 for reentrant geometry and Figure 3.21 for anti tetrachiral geometry.

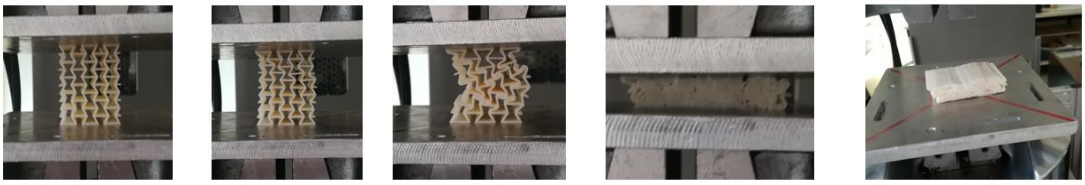

Figure 3.20: Step by step progress of the edge crush test of reentrant geometry.

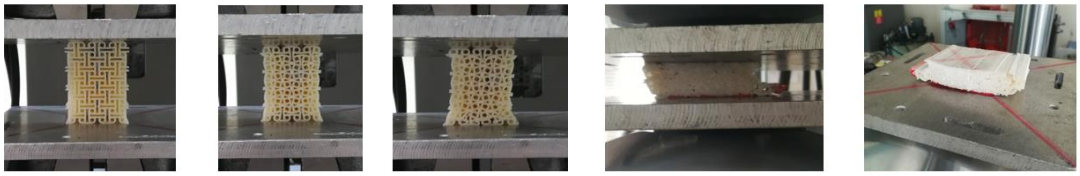

Figure 3.21: Step by step progress of the edge crush test of anti tetrachiral geometry.

It can be seen from the figures that, both geometries got denser with the time. This is not just the effect of compressing the material. Auxetic effect is more evident in the anti tetrachiral shape. As the time passes the gaps between cells got smaller and smaller, and width of the specimen decreased. This effect helped the material to become robuster. This effect can also be seen in the Figure 3.22. Red line represents the reentrant geometry, where green line represents the anti tetrachiral geometry. Axial force increased for both specimens with time. But the negative Poisson's Ratio was seen better on the anti tetrachiral structure.

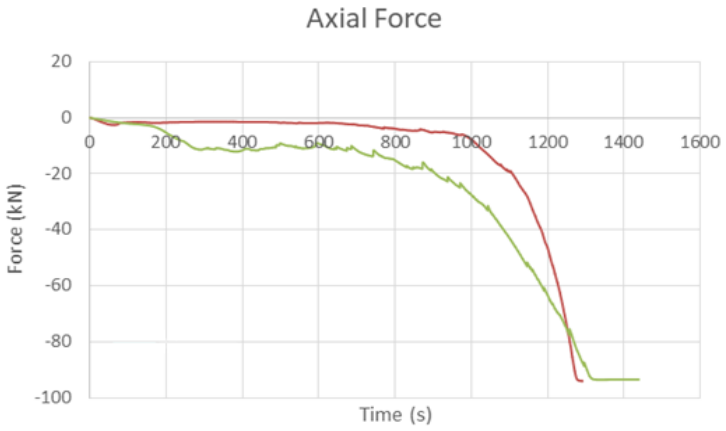

Figure 3.22: Axial force vs time. Red line for reentrant geometry, green line for anti tetrachiral geometry.

The auxetic effect is very clear at the anti tetrachiral geometry. It was seen in the visual inspection that, the material gathers as the time passes. Hence the resistance of the overall structure was expected to increase. If the graphical result is inspected, the gradual increase of the applied force can be seen. This is caused by the auxetic effect,

which causes material to resist the load together. The auxetic material accumulates together and creates a stronger material with increasing load.

The auxetic behaviour of the anti tetrachiral geometry is proved with the visual and graphical demonstrations. On the other hand, the auxetic effect was very week for the reentrant geometry. The main problem of this may be the misalignment of the specimen. The deformation was not well distributed, and the fracture started to move along the diagonal. This fracture movement also tilted the specimen and prevented it from showing the auxetic behaviour.

3.5 Comparison Between Numerical and Experimental Tests

Numerical analyses become more reliable after coupon tests. Actual material properties are defined in the software to get better results. Anti tetrachiral and reentrant structures are analysed both numerically and experimentally under impact loading. Hence, the comparison between analyses are done according to these tests.

The final stages of experiment and numerical analyses can be seen in Figure 3.23 for anti tetrachiral. Side view of the same structure's numerical analysis can also be seen in Figure 2.26.

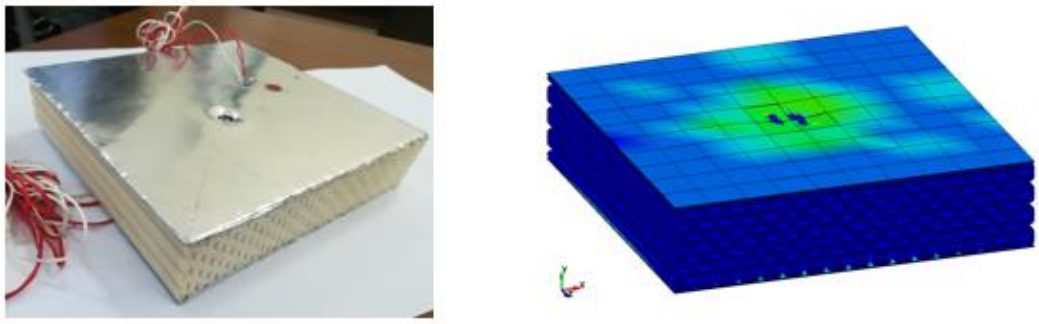

Figure 3.23: Side by side comparison of experimental and numerical comparison of the sandwich structure with anti tetrachiral core.

It was clear from the side view that the particle did not moved inside the core part, it only pierced the outer aluminium layer. The same situation was seen in the experimental test. The particle only hit the outer surface without damaging the core part too much. The particle moved 2.7 mm in experimental test and 1.8 mm in numerical analysis. The difference is possibly caused by the error of the either material properties or contact types defined in the analysis.

The results of the sandwich structure with reentrant core can be seen in Figure 3.24. Side view of the analysis is given in Figure 2.22. The particle moved inside the core 13.2 mm in numerical analysis, on the other hand this value occurred in the experimental test as 12.5 mm. The difference between these values are in the acceptable range.

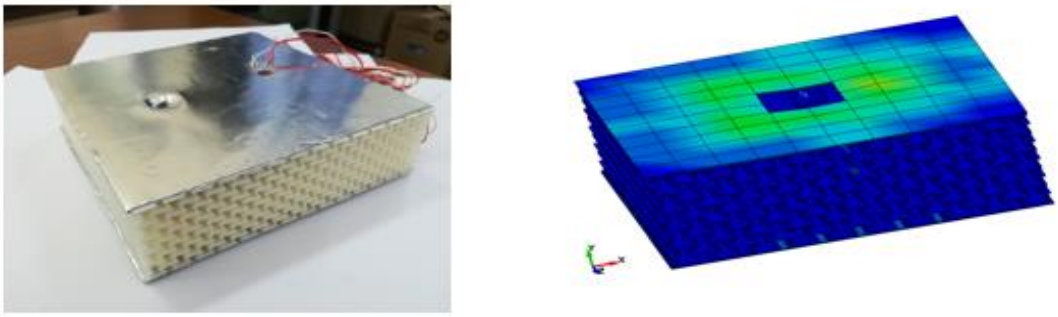

Figure 3.24: Side by side comparison of experimental and numerical comparison of the sandwich structure with reentrant core.

In Figure 3.25, strain values obtained from the numerical analysis can be seen. Strain gauge was also attached to the specimen to get the strain values occurred during the impact. Strain values of the experimental analysis can be seen in Figure 3.26. Both strain values are in micro strain domain. Strain values were obtained from a safe distance apart from the impact point. There is a strong similarity between experimental and numerical analyses.

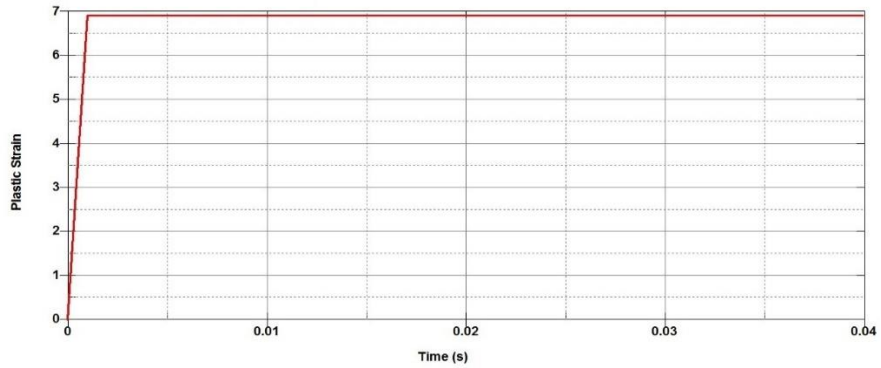

Figure 3.25: Strain values obtained from numerical analysis.

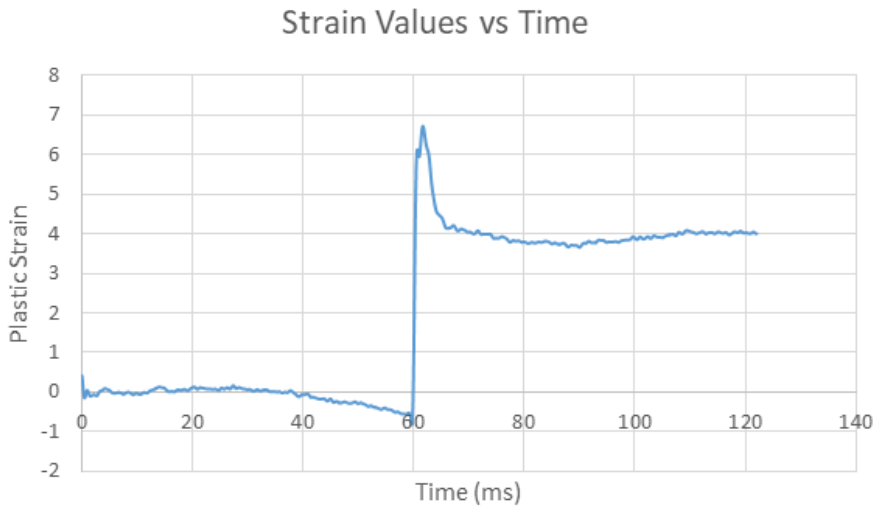

Figure 3.26: Strain values obtained from experimental test.

The time delay between the two figures can be explained by starting point. Since the strain gauge in real life starts recording before the experiment starts, region of zeroes may occur at the beginning of the recording. However, the strain recording can be adjusted to the starting point of the impact in the computer analysis. This causes a time delay between two strain recordings. Another difference between two sets of strain data is the region after the impact. A drop in the strain value occured on the experiment result, where strain value remained same throught the process on the numerical analysis. Main reason of this difference is the smoothness of the analysis. Movements and the contacts between each part are much smoother and animated than experimental results. And also, the computer analyses can reflect the real life experiments up to a point.

The tools required to perform the experimental tests were introduced in this chapter. Experimental tests started with determining the material properties of used materials. These properties were used in the numerical analyses, in order to make them more realistic. After that, impact tests were performed on sandwich structures with auxetic core. Even though honeycomb structure was not produced and tested, other expreriment results showed that numerical analyses values are valid. Hence, the comparison between honeycomb and reentrant structures are valid.

4. CONCLUSIONS AND RECOMMENDATIONS

Main focus of this thesis was to investigate the behaviour of auxetic materials. Two different auxetic geometries was selected in this manner. Both of the auxetic structures are proved to have the negative Poisson's Ratio. After the verification analyses, compression analyses were done on the anti tetrachiral core to see the response of the structure. As a result of the analyses, the cell dimensions of the anti tetrachiral core was improved and a denser structure was produced for the upcoming analyses. Reentrant, honeycomb and enhanced anti tetrachiral structures were analysed under impact loading. A convenient honeycomb geometry was selected according to the dimensions of the auxetic plate. Due to the financial issues, only auxetic structures were produced and tested under the same conditions. Honeycomb structure's result was obtained through the numerical analysis. At the final step a comparison between reentrant and honeycomb structures was made. Also, numerical and experimental results were compared with each other for validation.

The analyses of the auxetic materials and the conventional materials were done according to different loading situations, different boundary conditions and different angles. Both of the geometries behaved diversely to each of the conditions. Auxetic materials are very promising especially for the impact loadings.

The comparison between honeycomb and reentrant geometries showed that the structure can be strengthened by adjusting the cell structure. The length of the edges of the reentrant and honeycomb structures are same, 5.774 mm. However, changing the orientation of the edges creates an auxetic structure, which is thougher than conventional structure. This conclusion was made with the help of the stress values occurred during the impact analysis, 78.45 MPa for honeycomb and 47.15 MPa for reentrant structure. As explained above, the particle travelled less distance inside of the reentrant core than the honeycomb core. These two comparisons showed that auxetic structure resisted the impact loading better than conventional structure.

At the impact loading, auxetic material helped to protect the overall quality of the specimen. Honeycomb cored sandwich structures were damaged more under same loading condition, while auxetic cored sandwich plates resisted more to the impact loading and protected the original shape of the structure with the help of the unique geometrical properties of the structure.

4.1 Practical Application

Due to the unique ability of auxetic materials, they can be used widely. For example the outer surface of a tank can be covered with an extra layer of auxetic material to improve the blast loading resistance of the vehicle and it may help to save people inside the vehicle. Another application area of auxetic materials in the vehicle field may be crash box. Unfortunately, incidents and accidents with fatal casualities occur more frequently than desired. Moreover, they cause too many serious injuries or even death. The energy absorbation ability of the auxetic material can be a key point for the car accidents. Auxetic materials can be placed to absorb the kinetic energy of the car when the crash occurs.

The deformation behaviour of the auxetic materials can also be used in the Aeronautical field, as the deformation mechanism allows the structure to withstand more and more load. The unique ability of the auxetic materials was also seen during the edge crush test. Especially anti tetrachiral geometry resisted more and more loads with each time step. Aerial vehicles encounters with different kinds of loads constantly. The divergent condition of the weather always creates different loading conditions. Auxetic materials may help to overcome these conditions even at the extreme situations.

Also composite materials can be strengthened by adding auxetic materials to the mixture. As explained above, auxetic fibers are expected to behave better than the normal fibers. Adding auxetic fibers to the composite creates a new material that is stronger than the composite without auxetic fibers.

Even further application areas exist for auxetic materials. Aeronautical field is always searching for new materials and geometries to improve the product quality. Auxetic materials can be an answer to some of the requirements of aeronautical field. For example, auxetic materials can be used to strengthen the wings with their deformation

mechanism. Moreover, one can obtain a mixture that has the best properties of both materials by combining the conventional and auxetic materials. For example, unequal deflection of upper and lower surface of a material can cause problems. However, by using conventional material on top surface, and auxetic material on bottom surface creates a unique mixture and the material will have equal deflection. As the deformation mechanisms of conventional and auxetic materials are different.

Produced auxetic geometries were restricted to these dimensions because of the 3D printer specifications. Additionaly, with a better 3D printer, auxetic materials can be produced with improved shape in order to have a better connection between each cell.

Further researches can be made by optimizing the cell dimensions, using other auxetic structures or employing other analyses methods. However, auxetic structures are very promising compared to the conventional structure.

REFERENCES

Alderson, A., & Alderson, K. L. (2007). Auxetic materials. *Proceedings of the Institution of Mechanical Engineers, Part G: Journal of Aerospace Engineering*, *221*(4), 565–575. https://doi.org/10.1243/09544100JAERO185

Alderson, K. L., Simkins, V. R., Coenen, V. L., Davies, P. J., Alderson, A., & Evans, K. E. (2005). How to make auxetic fibre reinforced composites. *Physica Status Solidi (B) Basic Research*, *242*(3), 509–518. https://doi.org/10.1002/pssb.200460371

Almgren, R. F. (1985). An isotropic three-dimensional structure with Poisson's ratio =-1. *Journal of Elasticity*, *15*(4), 427–430. https://doi.org/10.1007/BF00042531

Czarnecki, S., & Wawruch, P. (2015). The emergence of auxetic material as a result of optimal isotropic design. *Physica Status Solidi (B) Basic Research*, *252*(7), 1620–1630. https://doi.org/10.1002/pssb.201451733

Dirrenberger, J., Forest, S., & Jeulin, D. (2013). Effective elastic properties of auxetic microstructures: Anisotropy and structural applications. *International Journal of Mechanics and Materials in Design*, *9*(1), 21–33. https://doi.org/10.1007/s10999-012-9192-8

Evans, K. E. (2000). Auxetic materials: the positive side of being negative. *Engineering Science and Education Journal*, *9*(4), 148. https://doi.org/10.1049/esej:20000402

Evans, K. E., & Alderson, A. (2000). Auxetic materials: Functional materials and structures from lateral thinking! *Advanced Materials*, *12*(9), 617–628. https://doi.org/10.1002/(SICI)1521-4095(200005)12:9<617::AID-ADMA617>3.0.CO;2-3

Jiang, L., Gu, B., & Hu, H. (2016). Auxetic composite made with multilayer orthogonal structural reinforcement. *Composite Structures*, *135*(January), 23–29. https://doi.org/10.1016/j.compstruct.2015.08.110

Ma, Y., Scarpa, F., Zhang, D., Zhu, B., Chen, L., & Hong, J. (2013). A nonlinear auxetic structural vibration damper with metal rubber particles. *Smart Materials and Structures*, *22*(8), 084012. https://doi.org/10.1088/0964-1726/22/8/084012

Mir, M., Ali, M. N., Sami, J., & Ansari, U. (2014). Review of mechanics and applications of auxetic structures. *Advances in Materials Science and Engineering*, *2014*, 1–18. https://doi.org/10.1155/2014/753496

Qi, C., Yang, S., Wang, D., & Yang, L. J. (2013). Ballistic resistance of honeycomb sandwich panels under in-plane high-velocity impact. *The*

Scientific World Journal, *2013*. https://doi.org/10.1155/2013/892781

Ruzzene, M., & Scarpa, F. (2005). Directional and band-gap behavior of periodic auxetic lattices. *Physica Status Solidi (B) Basic Research*, *242*(3), 665–680. https://doi.org/10.1002/pssb.200460385

Schwerdtfeger, J., Wein, F., Leugering, G., Singer, R. F., Körner, C., Stingl, M., & Schury, F. (2011). Design of auxetic structures via mathematical optimization. *Advanced Materials*, *23*(22–23), 2650–2654. https://doi.org/10.1002/adma.201004090

Smith, W. A. (1991). Optimizing Electromechanical Coupling in Piezocomposites Using Polymers with Negative Poisson's Ratio, 661–666.

Stavroulakis, G. E. (2005). Auxetic behaviour: Appearance and engineering applications. *Physica Status Solidi (B) Basic Research*, *242*(3), 710–720. https://doi.org/10.1002/pssb.200460388

Subramani, P., Rana, S., Oliveira, D. V., Fangueiro, R., & Xavier, J. (2014). Development of novel auxetic structures based on braided composites. *Materials and Design*, *61*, 286–295. https://doi.org/10.1016/j.matdes.2014.04.067

CURRICULUM VITAE

Name Surname **:** Altuğ Ataalp

Place and Date of Birth **:** Çorlu/03.09.1992

E-Mail **:** ataalpa@itu.edu.tr

EDUCATION **:**

- **B.Sc.** **:** 2015, Istanbul Technical University, Aeronautical and Astronautical Faculty, Aeronautical Engineering

PROFESSIONAL EXPERIENCE AND REWARDS:

- 2017-2018 Research Assistant at Istanbul Technical University at the Aeronautical and Astronautical Faculty.

PUBLICATIONS, PRESENTATIONS AND PATENTS ON THE THESIS:

- **Ataalp A., Türkmen H. S., and Kazanci Z..** 2017: impulsive pressure response of sandwich plates with auxetic core. Recent Topics on Mechanics and Materials in Design, June 11-15, 2017 Albufeira,Portugal.